



Development of diarylpentadienone analogues as alpha-glucosidase inhibitor: Synthesis, *in vitro* biological and *in vivo* toxicity evaluations, and molecular docking analysis

Maryam Aisyah Abdullah^{a,1}, Yu-Ri Lee^{b,1}, Siti Nurulhuda Mastuki^c, Sze Wei Leong^c, Wan Norhamidah Wan Ibrahim^{c,d}, Muhammad Alif Mohammad Latif^e, Aizi Nor Mazila Ramli^f, Mohd Fadhlizil Fasihi Mohd Aluwi^f, Siti Munirah Mohd Faudzi^{a,c,*}, Cheol-Hee Kim^{b,*}

^a Department of Chemistry, Faculty of Science, Universiti Putra Malaysia, 43400 UPM Serdang, Selangor, Malaysia

^b Department of Biology, Chungnam National University, 99 Daehak-ro, Yuseong-gu, Daejeon 34134, South Korea

^c Laboratory of Natural Products, Institute of Bioscience, Universiti Putra Malaysia, 43400 UPM Serdang, Selangor, Malaysia

^d Department of Biology, Faculty of Science, Universiti Putra Malaysia, 43400 UPM Serdang, Selangor, Malaysia

^e Department of Chemistry, Centre of Foundation Studies for Agricultural Science, Universiti Putra Malaysia, 43400 UPM Serdang, Selangor, Malaysia

^f Faculty of Industrial Sciences & Technology, Universiti Malaysia Pahang, Lebuhraya Tun Razak, Gambang, Kuantan, 26300 Pahang, Malaysia

ARTICLE INFO

Keywords:

Diarylpentadienones
Sulfonamide
 α -glucosidase inhibitor
Zebrafish
Molecular docking

ABSTRACT

A series of aminated- (1–9) and sulfonamide-containing diarylpentadienones (10–18) were synthesized, structurally characterized, and evaluated for their *in vitro* anti-diabetic potential on α -glucosidase and DPP-4 enzymes. It was found that all the new molecules were non-associated PAINS compounds. The sulfonamide-containing series (compounds 10–18) selectively inhibited α -glucosidase over DPP-4, in which compound 18 demonstrated the highest activity with an IC_{50} value of $5.69 \pm 0.5 \mu M$ through a competitive inhibition mechanism. Structure-activity relationship (SAR) studies concluded that the introduction of the trifluoromethylbenzene sulfonamide moiety was essential for the suppression of α -glucosidase. The most active compound 18, was then further tested for *in vivo* toxicities using the zebrafish animal model, with no toxic effects detected in the normal embryonic development, blood vessel formation, and apoptosis of zebrafish. Docking simulation studies were also carried out to better understand the binding interactions of compound 18 towards the homology modeled α -glucosidase and the human lysosomal α -glucosidase enzymes. The overall results suggest that the new sulfonamide-containing diarylpentadienones, compound 18, could be a promising candidate in the search for a new α -glucosidase inhibitor, and can serve as a basis for further studies involving hit-to-lead optimization, *in vivo* efficacy and safety assessment in an animal model and mechanism of action for the treatment of T2DM patients.

1. Introduction

Diabetes mellitus or diabetes has become an increasing problem worldwide, both in rich and poor countries. It is a chronic and progressive disease associated with elevated glucose levels in the blood and is known as hyperglycaemia if the condition persists over a prolonged period. Over time, diabetes may lead to complications such as heart attack, stroke, kidney failure, leg amputation, vision loss, and nerve damage [1]. Most diabetes patients are affected by type 2 diabetes mellitus (T2DM), a metabolic disorder that is often coupled with insulin resistance that affects the way the body metabolises its important

source of fuel, glucose [2]. As reported by the International Diabetes Federation (IDF), T2DM comprises approximately 90% of all cases of diabetes, and to date, it is estimated that 15 million people are affected globally [3]. Previously, T2DM had only been diagnosed in older adults, but surprisingly, the current statistics show that T2DM is becoming more prevalent among children and adolescents due to escalating obesity and overweight incidences among the youth [1]. While current T2DM therapies involving the increase of insulin secretion have shown therapeutically beneficial effects, these are often accompanied by undesirable side effects such as hypoglycaemia and weight gain. Due to the reported adverse side effects, most of these treatments are

* Corresponding authors at: Laboratory of Natural Products, Institute of Bioscience, Universiti Putra Malaysia, 43400 UPM Serdang, Selangor, Malaysia.

E-mail addresses: sitimunirah@upm.edu.my (S.M. Mohd Faudzi), zebrakim@cnu.ac.kr (C.-H. Kim).

¹ These authors contributed equally.

unsatisfactory with regards to the prevention of complications and preservation of quality of life [4]. Thus, there is a significant medical need for the discovery of new and effective anti-diabetic agents for the treatment of T2DM.

α -Glucosidase is an enzyme that catalyses the final steps in the digestion of carbohydrate; hence, α -glucosidase inhibitors could retard the catabolism of dietary carbohydrates to suppress postprandial hyperglycaemia. There are arguments that α -glucosidase inhibitors such as acarbose (Glucobay) and miglitol (Glyset), although effective in decreasing the absorption of glucose by interfering with the action of α -glucosidases in the small intestinal mucosa, are often associated with abdominal bloating, diarrhoea, and flatulence [5]. α -Glucosidase inhibitors also raise post-meal levels of glucagon-like peptide-1 (GLP-1), an incretin hormone secreted by the intestine following the ingestion of various nutrients to stimulate insulin secretion and inhibit glucagon release, which slows the gastric emptying process and suppresses appetite [6]. This means that they do not increase the likelihood of weight gain, unlike sulfonylureas and thiazolidinediones [7].

Since 2006, dipeptidyl peptidase-4 (DPP-4) inhibitors have become a new class of agents that are proven to be an effective treatment of diabetes by improving glycaemic control [8]. DPP-4 inhibitors target DPP-4, a serine protease enzyme which deactivates two potent stimulators of insulin secretion, GLP-1, and glucose-dependent insulinotropic polypeptide (gastric inhibitory polypeptide or GIP) [9]. Like GLP-1, GIP also helps to delay digestion and decrease appetite. However, both hormones are rapidly cleaved to their inactive forms by the enzyme DPP-4, thus, reducing their potency in preventing diabetes-related complications. Therefore, it is important to note that inhibition of DPP-4 is compulsory to increase levels of endogenous incretin hormones GLP-1 and GIP for the treatment of diabetes [10].

Chalcone is a small bioactive molecule composing of 1,3-diarylprop-2-en-1-one framework and is one of the abundant secondary metabolites of terrestrial plants and precursors of flavonoid biosynthesis [11–13,33]. These molecules have been receiving great attention by the scientific community due to its simple chemistry, ease of synthesis, diversity of substituents, safety, and a vast number of recognized biological activities, including anti-obesity, anti-hypertensive and anti-diabetic activities [13–15]. Several reports even indicate that chalcones may inhibit the enzymes α -amylase [16–19] and α -glucosidase [16,20–24]. Seo et al. (2005) reported aminated series of chalcone exhibited greater inhibition of three glycosidase enzymes (α -glucosidase from baker's yeast, α -amylase from *Bacillus licheniformis* and β -amylase from barley) over other chalcone derivatives. The α -glucosidase inhibitory was then improved progressively when the aminated series were chemically modified into sulfonamide chalcones, which shown 150-fold stronger suppression than acarbose [25].

Sulfonamide, too, has received a lot of attention and is used as an intermediate functional group in many therapeutic drugs [26]. Several synthetic pharmacological agents that consist of a sulfonamide group possess anti-bacterial [27], antimalarial [28], diuretic [29], anti-rheumatic [30], and anti-retroviral properties [31]. Previous studies also reported that sulfonamide-containing compounds are essential for DPP-4 inhibitory activity [32].

Moreover, Rocha et al. (2019) investigated the effect of an extra double bond on the enone linker chain of the synthesized chalcone derivative, the diarylpentadienone against α -glucosidase [33]. Results revealed a slight improvement in the inhibitory activity of diarylpentadienones when compared to its chalcone derivative and the standard α -glucosidase inhibitor (AGI), acarbose. Recently, researchers have discovered diarylpentadienone analogues along with their various pharmacological activities, including promising anti-inflammatory property, significant anti-cancer effect towards leukaemia and breast cancer, excellent anti-microbial, anti-fungal, and anti-rhinovirus properties, and as an effective antioxidant [34–39]. Despite the numerous

bioactivities of diarylpentadienone derivatives, to the best of our knowledge, there is very little scientific information with regards to their potential as an anti-diabetic drug.

Thus, in continuation of our endeavors toward exploration of the therapeutic potential and clinical implication of diarylpentadienones particularly as α -glucosidase and DPP-4 inhibitors, we herein report the design, synthesis, *in vitro* biological evaluation, toxicity profiling using zebrafish *in vivo* animal model, and molecular docking of a new series of integrated sulfonamide-containing diarylpentadienones as potential anti-diabetic agents for the treatment of T2DM.

2. Results and discussions

2.1. Pan-assay interference compounds (PAINS) and aggregator identification

PAINS is defined as a substance with reactive structural cores that may give false-positive results in biological assays due to several mechanisms, including protein binding interactions [40] and the formation of colloidal aggregates [41]. Scientific manuscripts primarily reporting on the activity and therapeutic utility of curcuminoids and chalconoids-related compounds are regularly published and has caught the attention of the scientific community. Chalconoids, a derivative of curcumin has been previously reported as a PAINS-associated class of compounds due to its reactive α,β -unsaturated ketone linker moiety. In order to avoid any misleading information, the identification of any PAINS-containing molecules in the newly designed bioactive candidates prior to the synthesis work has become a crucial step to validate that the function of a compound is as expected. In view of this, we input all 18 newly designed diarylpentadienones and its derivatives into publicly available filter servers, FAF-Drugs4 [42] and Aggregator Advisor [43] for PAINS and aggregator identification, respectively.

Based on the PAINS identification analysis, none of the newly synthesized molecules were PAINS-associated compounds (see Supporting Information). Likewise, through *the in-silico* aggregator prediction analysis, none of the compounds were similar to any known aggregator. However, all molecules (compounds 1–18) were predicted with a highly calculated LogP (3.4 to 6.7) and may be potential aggregates. The respective LogP range (> 3) was previously reported in many other aggregators [44].

To test this prediction, we intended to investigate aggregation in the identified prominent α -glucosidase inhibitor **18** (as discussed in Section 2.3) via centrifugation counter-screen technique [45]. However, due to sample availability and a complex purification of **18**, we, therefore, use its *ortho*-analogue **16** as the tested compound. Theoretically, this method induces the formation of pellets originating from aggregates, leaving only the monomeric compound in the post-centrifugation supernatants as illustrated in Fig. 1, and thus lowering the bioactivity when compared to pre-centrifugation tested sample [46,45].

As depicted in Fig. 2, the recorded α -glucosidase inhibitory activities of pre- and post-centrifuged supernatants of **16** was almost comparable with IC_{50} of $8.56 \pm 2.3 \mu M$ and $9.92 \pm 2.3 \mu M$, respectively. These results herein verify that the inhibitory property of **16** did not attribute to the formation of the aggregates, which indirectly gave a hint of the non-aggregate characteristic of **18**.

In this study, we particularly would like to reinforce the importance of identifying artifactual aggregates as a fundamental step in experimental validation to avoid promiscuous inhibition that may lead to false-positive bioactivity [44,47–49]. This can be achieved by performing the computational predictions and accurate experimental procedures to control for aggregation in minimizing the impact of this important issue in drug design. Regrettably, only a few studies have directly addressed this issue in the published literature.

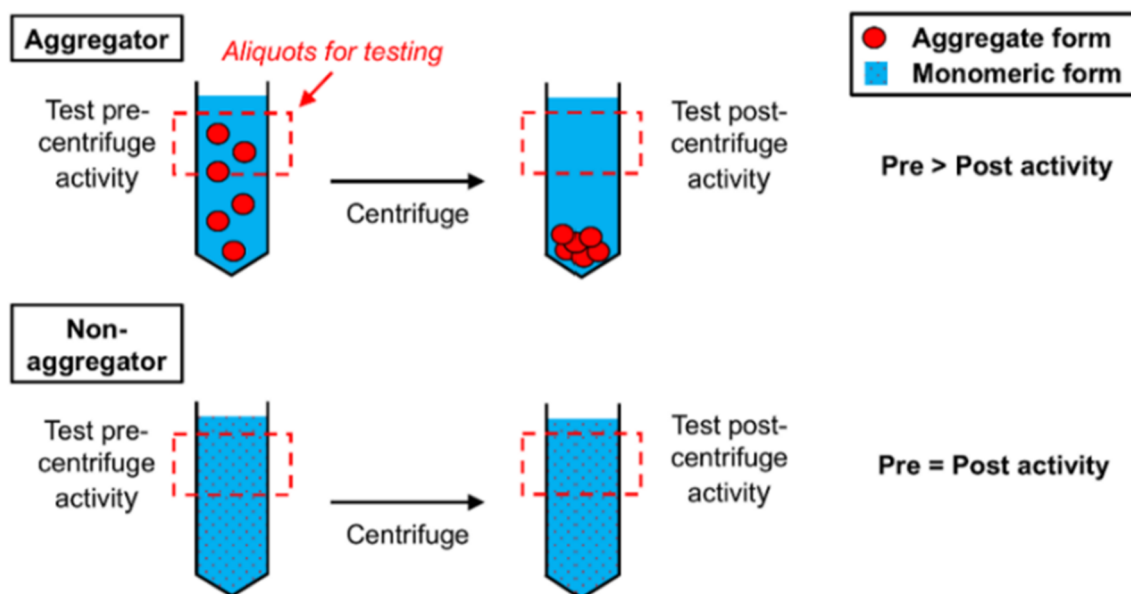


Fig. 1. Aggregates (top panel) can be removed via centrifugation of samples. If the post-centrifugation supernatant aliquots show reduced inhibitory activity compared to the pre-centrifugation sample, the compound is suspected to be an aggregator. In contrast, non-aggregators (bottom panel) recorded similar bioactivity on pre- and post-centrifugation tested samples [45].

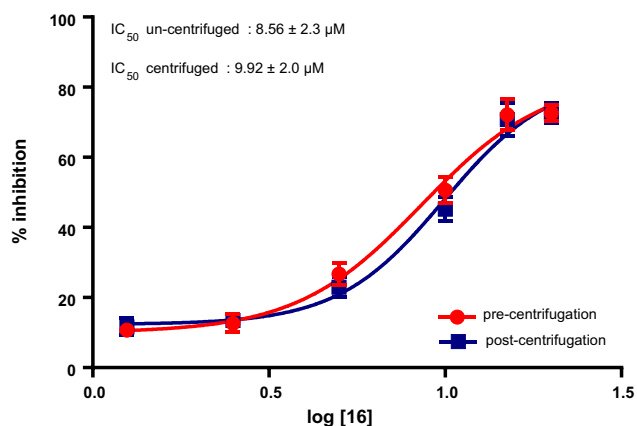
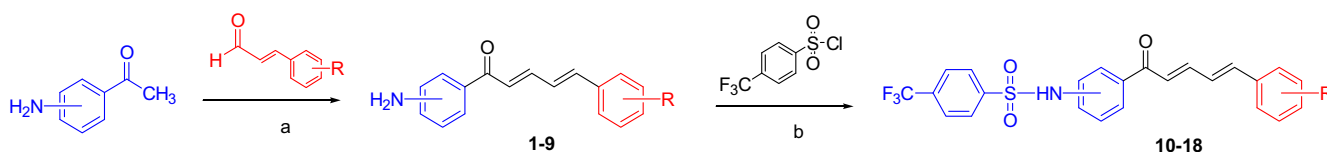


Fig. 2. Dose-response curves of 16 to determine aggregate formation using centrifugation counter-screen technique.

2.2. Chemistry

The aminated-diarylpentadienones (1–9) were synthesized via Claisen-Schmidt condensation of the appropriate cinnamaldehydes and aminoacetophenones in the presence of a catalytic amount of NaOH. Further sulfonylation reaction between compounds 1–9 and *p*-trifluoromethylbenzenesulfonyl chloride to afford sulfonyl-containing diarylpentadienones (10–18) is described in Scheme 1. All the synthesized compounds were purified by flash chromatography and recrystallization techniques and were structurally characterized by spectroscopic analyses, including the 1H and ^{13}C NMR, Fourier



Scheme 1. General synthetic step for compounds 1–18. Reagents and conditions: (a) amino-acetophenone, 6 M NaOH, EtOH, RT (overnight), (b) *p*-trifluoromethylbenzenesulfonyl chloride, pyridine, MeOH, RT (overnight).

Transform Infra-Red (FTIR), and Direct Infusion-Mass Spectrometry (DIMS).

The 1H NMR spectra of all aminated-diarylpentadienone analogues exhibited a moderate and broad singlet at 5–7 ppm, indicative of primary amine groups. The signal becomes weaker after the introduction of sulfonamide moiety. DIMS and FT-IR results further verify that all the compounds were successfully synthesized. The molecular ion peak detected in each DIMS spectrum was compatible with their respective molecular formula. For instance, the IR spectra of compounds 1–9 show a weak band at $3100\text{--}3300\text{ cm}^{-1}$ and a strong band at $1500\text{--}1600\text{ cm}^{-1}$ due to the N–H and C=O stretching vibrations, respectively. Meanwhile, compounds 10–18 shows a weak band around $3100\text{--}3300\text{ cm}^{-1}$ due to the N–H stretching of a secondary amine and $1500\text{--}1600\text{ cm}^{-1}$ due to the C=O stretching vibrations. Two strong absorption bands were observed around 1200 and 1000 cm^{-1} , indicating the asymmetric and symmetric stretching peak of the SO_2 group.

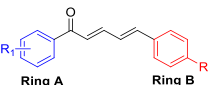
It was observed, with the use of the Claisen-Schmidt condensation reaction carried out at room temperature overnight, that low amounts of crude aminated-diarylpentadienones (1–9) were produced at approximately 7% – 40% yield. Under these conditions, the possibility of the Cannizzaro reaction taking place simultaneously was considered, thereby decreasing the yield of the desired product [50].

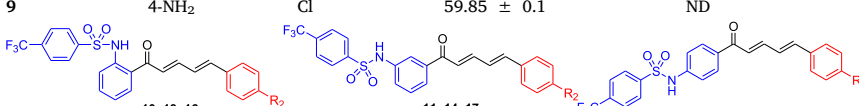
2.3. In vitro α -glucosidase and DPP-4 inhibition activities

Eighteen purified diarylpentadienone derivatives (1–18) were firstly screened *in vitro* against α -glucosidase and DPP-4 enzymes at 50 μM and 100 μM test concentrations, respectively. Based on the preliminary evaluation, nine compounds (10–18) were significantly

Table 1

α -Glucosidase and DPP-4 suppression of the tested diarylpentadienone derivatives 1–18. Data are presented as mean \pm SEM, and $n = 3$



Compound	R ₁ (Ring A)	R ₂ (Ring B)	α -Glucosidase ^a		DPP-4 ^a	
			Inhibition at 50 μ M (%)	^a IC ₅₀ (μ M) \pm SEM	Inhibition at 100 μ M (%)	^b IC ₅₀ (μ M) \pm SEM
1	2-NH ₂	H	4.27 \pm 0.2	ND	70.20 \pm 2.0	26.91 \pm 2.3
2	3-NH ₂	H	59.60 \pm 0.1	ND	26.85 \pm 0.7	ND
3	4-NH ₂	H	36.65 \pm 0.1	ND	68.78 \pm 4.2	ND
4	2-NH ₂	OMe	37.21 \pm 0.2	ND	68.40 \pm 5.9	ND
5	3-NH ₂	OMe	24.07 \pm 0.1	ND	31.11 \pm 10.0	ND
6	4-NH ₂	OMe	24.10 \pm 0.2	ND	44.48 \pm 3.6	ND
7	2-NH ₂	Cl	20.61 \pm 0.2	ND	37.75 \pm 3.2	ND
8	3-NH ₂	Cl	54.02 \pm 0.1	ND	46.10 \pm 3.0	ND
9	4-NH ₂	Cl	59.85 \pm 0.1	ND	70.02 \pm 1.6	79.02 \pm 2.9
						
10		H	95.56 \pm 5.1	6.29 \pm 0.9	72.76 \pm 0.5	54.08 \pm 4.4
11		H	83.10 \pm 1.6	7.16 \pm 0.5	47.96 \pm 3.9	ND
12		H	92.61 \pm 2.6	8.63 \pm 4.4	48.33 \pm 3.7	ND
13		OMe	94.35 \pm 3.7	14.04 \pm 1.2	62.38 \pm 5.0	ND
14		OMe	96.91 \pm 1.7	11.69 \pm 0.9	71.52 \pm 0.9	33.67 \pm 0.8
15		OMe	93.99 \pm 9.1	12.16 \pm 2.1	75.49 \pm 2.9	17.81 \pm 0.3
16		Cl	98.80 \pm 1.2	8.56 \pm 2.3	66.68 \pm 2.8	ND
17		Cl	97.17 \pm 3.5	7.21 \pm 0.4	58.59 \pm 2.2	ND
18		Cl	99.16 \pm 7.5	5.69 \pm 0.5	53.46 \pm 3.2	ND
	Acarbose [*]		97.79 \pm 0.1 [*]	0.22 \pm 0.1 [*]		
	Sitagliptin ^{**}		–	–	88.48 \pm 3.1	0.07 \pm 0.1

ND = Compound is not determined

^{*} Standard drug used for α -glucosidase inhibitory assay, screened at initial concentration of 3.91 μ M

^{**} Standard drug used for DPP-4 inhibitory assay

^a IC₅₀ determination was conducted for compounds of > 80% α -glucosidase inhibition

^b IC₅₀ determination was conducted for compounds of > 70% DPP-4 inhibition

[#] The IC₅₀ graph of the respective compounds can be found in the Supporting Information

inhibited at > 80% α -glucosidase, whereas five analogues (1, 9, 10, 14, and 15) were shown to exhibit good suppression at > 70% on DPP-4 enzyme, indicating that these new diarylpentadienones may potentially possess anti-diabetic properties. The IC₅₀ values of fourteen bioactive compounds were further determined and were compared to the standard anti-diabetic drugs, acarbose and sitagliptin, respectively. The overall inhibitory effects of α -glucosidase and DPP-4 towards the aminated- and sulfonylated-diarylpentadienones (1–18) are tabulated in Table 1.

The α -glucosidase bioassay was conducted using α -glucosidase from *Bacillus stearothermophilus* as the target enzyme according to the protocol in optimal conditions [51,52]. Acarbose was used as a standard positive control in this *in vitro* assay for activity comparison. From the results obtained, the aminated-diarylpentadienones (1–9) showed lower percentages of α -glucosidase inhibition compared to the sulfonamide-containing series (10–18) and were too inactive than acarbose. This observation might have been due to the higher basicity of the primary amino group of compounds 1–9, which may have reduced the inhibitory activity, regardless of the position of the amino moiety on phenyl Ring A (*ortho/meta/para*).

On the other hand, it is interesting to note that the α -glucosidase suppression ability was enhanced significantly with the IC₅₀ values ranging from 5.69 to 12.16 μ M when the sulfonamide moiety was introduced on Ring A, regardless of the *ortho*, *meta*, and *para* positioning. The result of the α -glucosidase suppression screening showed that compound 18 displayed significant α -glucosidase inhibitory activity with IC₅₀ values of 5.69 \pm 0.5 μ M in a dose-dependent manner (Fig. 3), however, the potency was 27-folds lower to acarbose (IC₅₀ value of 0.21 \pm 0.1 μ M). Whereas, compounds 10 (IC₅₀ = 6.29 \pm 0.9 μ M), 11 (IC₅₀ = 7.16 \pm 1.6 μ M), 12

(IC₅₀ = 8.63 \pm 4.4 μ M), 13 (IC₅₀ = 14.04 \pm 1.2 μ M), 14 (IC₅₀ = 11.69 \pm 0.9 μ M), 15 (IC₅₀ = 12.16 \pm 2.1 μ M), 16 (IC₅₀ = 8.56 \pm 2.3 μ M) and 17 (IC₅₀ = 7.21 \pm 0.4 μ M) have progressively improved the α -glucosidase inhibitory activity compared to their parent aminated-diarylpentadienones (compounds 1–9), which is further verifying the importance of the sulfonamide. The O=S=O of the trifluoromethylbenzene sulfonamide (*p*-CF₃C₆H₄SO₂) group might contribute to the increase in the hydrogen bonding capabilities of the bioactive molecules towards α -glucosidase enzyme, coupled with the reducing basicity of the sulfonamide moiety, which has ultimately improved the targeted bioactivity (the interactions will be discussed in detail in Section 2.5).

Following that, we investigated the impacts of substituents with different electronic properties on Ring B of the sulfonamide-containing diarylpentadienone series, which was responsible for the varying degrees of anti-diabetic potency. Interestingly, the lower electron density, *p*-chloro-substituted and unsubstituted phenyl on ring B compounds (10–12 and 16–18) demonstrated slightly higher α -glucosidase inhibition than the *p*-methoxy-substituted (13, 14, and 15) analogues. It is therefore suggested, through this preliminary works, that the presence of electron-withdrawing groups or a lower electron density moiety (e.g., halogens) on Ring B accompanied with the sulfonamide group on Ring A of diarylpentadienone scaffold are the features that were responsible towards significant α -glucosidase inhibition.

In addition, we compared the effects of *ortho*-, *meta*-, and *para*-substitution of sulfonamide on the Ring A feature towards α -glucosidase suppression. It was apparent that the *para*-sulfonamide substituted compound 18, together with the *para*-chloro group on Ring B, showed higher inhibitory activity, whereas the *ortho*- and *meta*-sulfonamide substituted analogues exhibited a slightly lower yet comparable α -

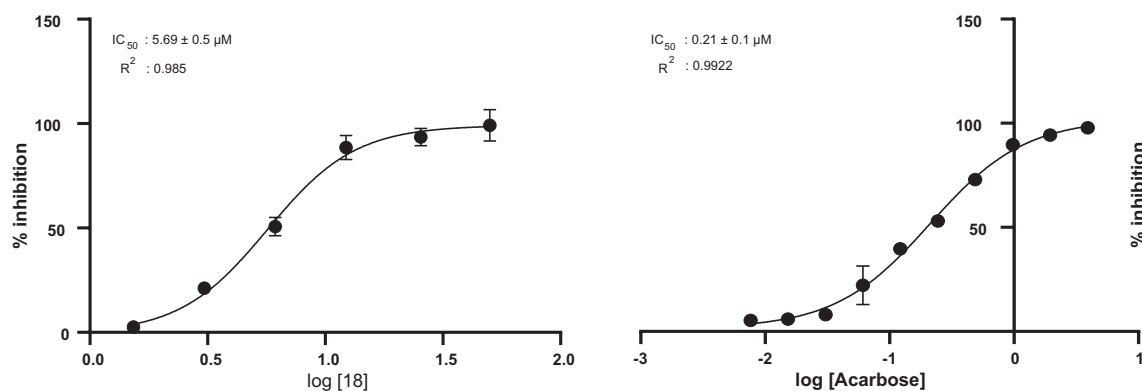


Fig. 3. Dose-response curve of compound **18** and acarbose on α -glucosidase inhibition.

glucosidase inhibition activity when Ring B was replaced with free phenyl and *para*-methoxyphenyl, respectively. These findings further confirmed the enhancing effect of *para*-substitution and the critical role of sulfonamide moiety in α -glucosidase inhibitory activity.

In summary, these results revealed that the nature of substituents on the phenyl ring B with different sulfonamide locations on ring A of the newly synthesized diarylpentadienones are closely associated with the biological activities of α -glucosidase inhibitors. This information gathered through structure–activity relationships (SAR) studies could potentially guide future structural modifications of these sulfonylated-diarylpentadienones for the improvement of α -glucosidase inhibitory activity, as well as to identify new leads with desirable inhibitory properties. In this regard, *para*-sulfonamide (Ring A) and *para*-chloro were identified as the most important feature for α -glucosidase inhibitory activity.

Following the α -glucosidase *in vitro* assay, all the synthesized compounds were also assayed for DPP-4 inhibition activity to explore the potential of diarylpentadienones towards different target enzymes responsible for diabetes or T2DM. The standard drug, sitagliptin was used as a positive control in the respective assays. Among all the derivatives, compound **15** exhibited the highest activity in this series with IC_{50} values of $17.81 \pm 0.3 \mu\text{M}$. However, this compound showed weaker activity by > 100 folds compared to the standard sitagliptin ($IC_{50} = 0.071 \pm 0.005 \mu\text{M}$). In brief, no SAR can be summarized throughout this finding, it is therefore suggested, further chemical modifications on the structural core is needed to establish this class of compound as new anti-DPP-4 agents.

2.4. Kinetic studies of **18** against α -glucosidase

The inhibition mechanism of the most active sulfonamide analogue **18** against α -glucosidase was deduced from the Lineweaver-Burk plot.

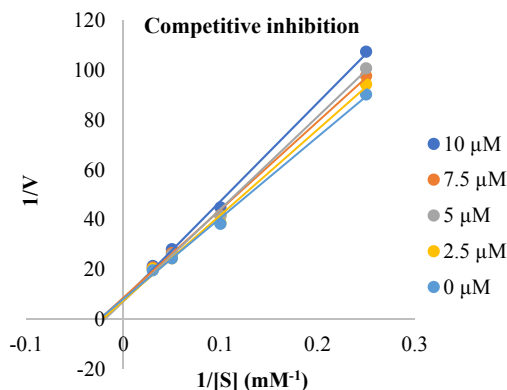


Fig. 4. Lineweaver-Burk plot analysis of the inhibition kinetics of α -glucosidase suppression effects by compound **18**.

The analysis was carried out by investigating the effects of inhibitors' concentration (0, 2.5, 5.0, 7.5, 10.0, 12.5, 15.0 and 20.0 μM) on enzyme activity at different concentrations of substrate (1.25, 2, 4, 10, 20 and 30 mM). As depicted in Fig. 4, analogue **18** behaved as a competitive inhibitor, as the K_m value increase and V_{max} remained constant with increasing concentrations of the compound.

2.5. *In vivo* toxicity test in zebrafish embryos

In the last two decades, the zebrafish has become extensively used as a toxicological model, in part due to their small size, rapid external development, short life cycle, high reproductive rate, and simple husbandry requirements [53]. This *in vivo* model has been routinely used to perform rapid risk assessments and regulations in addition to the measurements of therapeutic activities of compounds through *in vivo* approaches as it exhibits a diverse repertoire of biological processes and possesses a fully integrated vertebrate organ system [54,55].

In order to profile the toxic effects of compound **18** that showed promising potential as an α -glucosidase inhibitor, we treated zebrafish embryos with various dosages of the compound (1, 2, 5, 10, 20, and 40 μM) starting from 6 hpf via bath immersion. At 24 and 48 hpf, morphological comparisons were made between exposed embryos versus the control (Fig. 5) to observe any morphological deformities via an embryo acute toxicity test.

As shown in Fig. 5, the treated embryos were alive after exposure to compound **18** at 24 hpf and 48 hpf with no signs of morphological deformities. Results showed that embryos treated with compound **18** displayed similar body length, yolk extension, curve trunks, somite boundary, blood circulation, and pigment cell development compared to the control, reflecting the non-toxic properties of compound **18** up to 40 μM .

To further determine whether compound **18** may cause apoptosis or cell death at 10, 20, and 40 μM concentrations, the treated embryos were assessed using a vital fluorescent dye, acridine orange (AO) at 108 hpf to mark apoptotic cells. Apoptosis is a critical component of the normal developmental process in multiple tissues and organ systems. The process of apoptotic cell death is highly conserved and follows a morphologically distinctive pattern. Apoptosis can be described with specific cellular shrinkage, membrane blebbing, nuclear condensation and nuclear fragmentation that commonly recognized as hallmarks of this type of cell death [56]. The vital dye AO staining technique has been commonly applied for cell death monitoring in live animals, including zebrafish. Based on the results as depicted in Fig. 6, AO-positive cells were clearly and broadly detected throughout the bodies of the DMSO vehicle- and compound **18**-treated transgenic zebrafish at all tested concentrations. The results indicate that compound **18** has no negative interferences towards apoptosis in the developing zebrafish embryos as compared to the control.

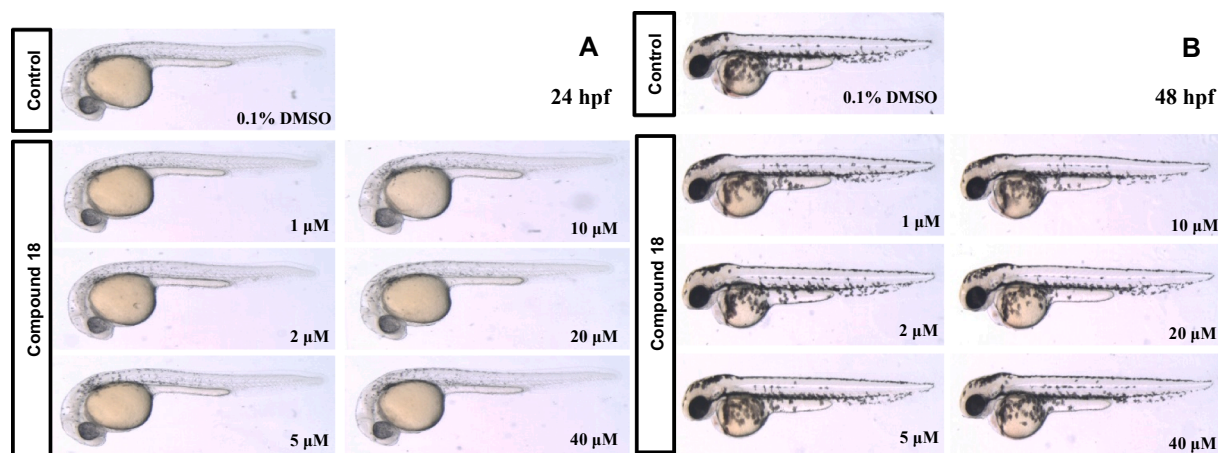


Fig. 5. Morphological features of zebrafish larvae at different developmental stages of (A) 24 hpf and (B) 48 hpf after exposure to compound 18 at various concentrations, 1, 2, 5, 10, 20, and 40 μM, respectively. Scale bars, 200 μm.

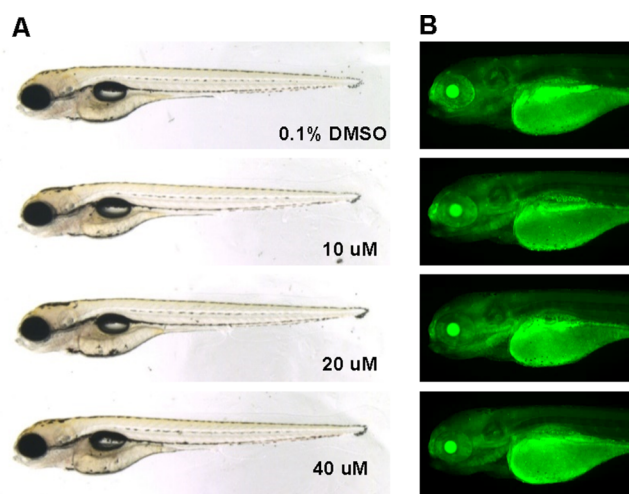


Fig. 6. (A) Effects of long-term exposure (4.5 days) of compound 18 on zebrafish larvae at different concentrations, 10, 20 and 40 μM, respectively. (B) Acridine orange staining for cell death. Signals in yolk and lens are autofluorescence. Scale bars, 200 μm. (For interpretation of the references to colour in this figure legend, the reader is referred to the web version of this article.)

Considering the conservation of the basic vascular pattern in different vertebrates, the signaling molecules and cellular mechanisms by which blood vessels form have been evolutionarily conserved [57]. Consequently, it is possible to gain significant insights into pathological blood vessel formation through the study of embryonic vascular

development in the vertebrate model system. Since blood vessel function is critical for vertebrate embryonic development [58], we further our investigations on the toxic effects of compound 18 by using a transgenic line of zebrafish that specifically expresses green fluorescent protein (GFP) in their vascular endothelial cells, *Tg(kdrl:egfp)* to delineate the normal development of the blood vessel. The late gastrula 10 hpf *Tg(kdrl:egfp)* zebrafish embryos were incubated with compound 18 in different concentrations of 10, 20, and 40 μM for a day and examined at 30 hpf under a fluorescent microscope. Compound 18 treatment up to 40 μM revealed no adverse effects on the normal development of vasculature, including intersegmental vessels (ISVs), as shown in Fig. 7.

2.6. Molecular docking studies

In order to gain functional and structural insights into the binding mode of the most active analogues into their respective protein, molecular docking was performed using AutoDockVina. Compound 18 was selected for the docking studies into the homology modeled α-glucosidase protein (PDB ID: 2ZE0) and human lysosomal acid α-glucosidase (GAA, PDB ID: 5NN8), whereas compound 15 was selected for the molecular interaction with DPP-4.

Since the crystal structure of the α-glucosidase from *Bacillus stearothermophilus* was unavailable at the time of writing, a homology model of the α-glucosidase was built according to a previously reported method for the molecular docking analysis. α-Glucosidase of *Bacillus subtilis* (PDB ID: 2ZE0) was chosen as the template for the respective homology model since it shared 98.7% identity and possesses a sequence similarity score of 0.62 with α-glucosidase of *Bacillus stearothermophilus* (Swissprot code P53341/P38158). The homologous

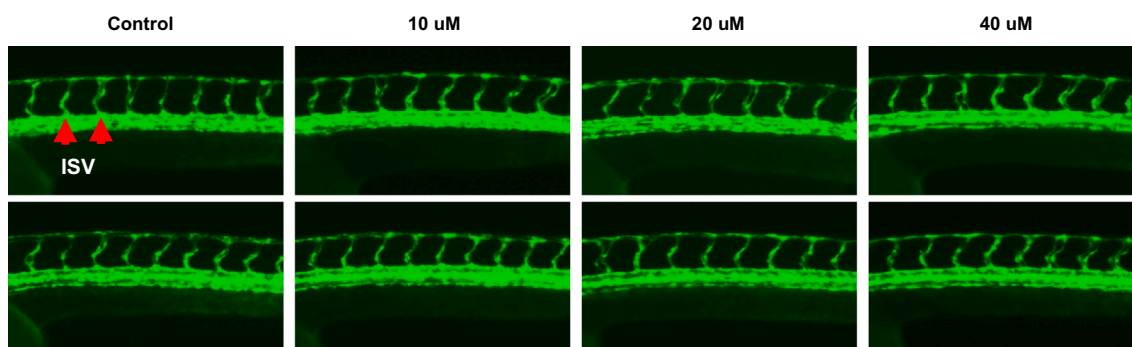


Fig. 7. Effects of compound 18 with different concentrations (10, 20, and 40 μM) on the blood vessel development in transgenic zebrafish, *Tg(kdrl:egfp)* at 30 hpf. Vasculogenesis and angiogenesis, including intersegmental vessels (arrows), in the trunk region were normal in both the untreated control and compound 18-treated zebrafish. Scale bars, 200 μm.

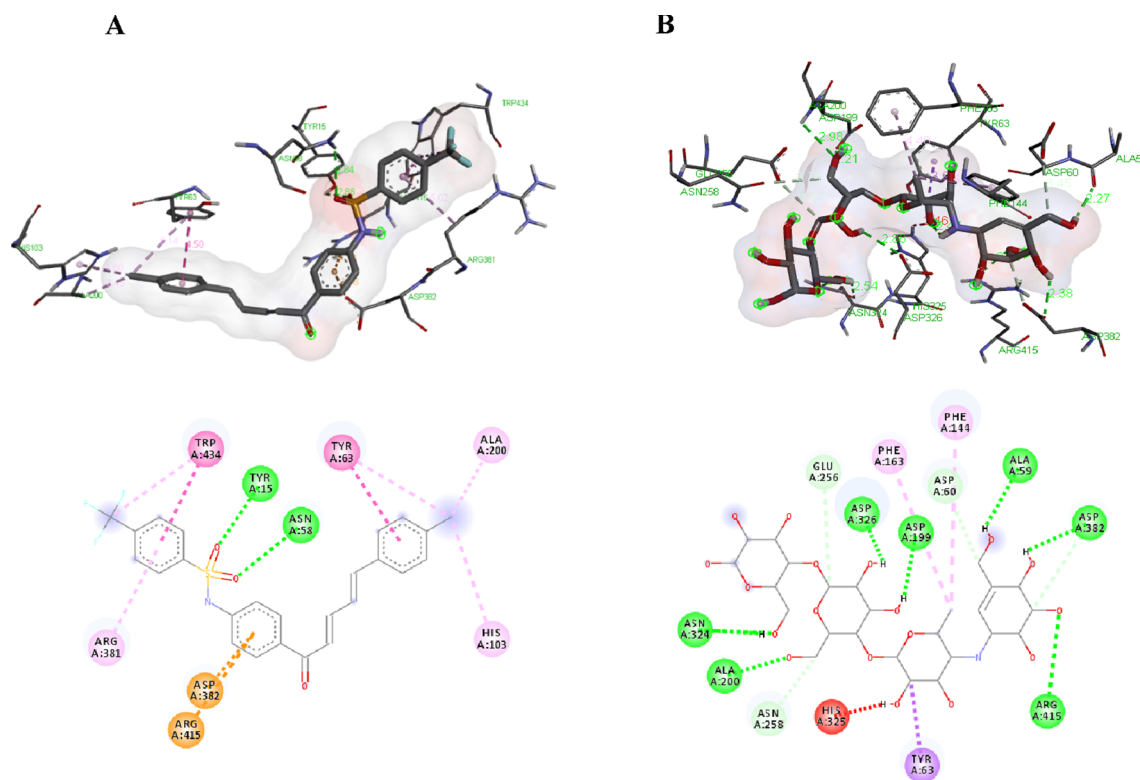


Fig. 8. 3D and 2D diagram of the binding interactions of (A) compound **18** and (B) acarbose with the active site residues of the α -glucosidase receptor. (Green line: H bond; orange line: π -cation/anion; purple line: π - π stacked/*T*-shaped; light purple: Alkyl/ π -Alkyl). (For interpretation of the references to colour in this figure legend, the reader is referred to the web version of this article.)

Table 2

Data of interactions resulting from the molecular docking of compounds **18** and acarbose into α -glucosidase.

Compound 18				Acarbose			
Active site	Interactions	With	Bonding distance (Å)	Active site	Interactions	With	Bonding distance (Å)
Tyr15	H bond	S=O	2.88	Ala200	H bond	O-H	2.98
Asn58	H bond	S=O	2.84	Asn324	H bond	O-H	2.296
Trp434	π -alkyl/ Alkyl	CF ₃	4.59	Arg415	H bond	O	2.26
	π - π <i>T</i> -shaped	Benzene (Phenyl sulfonamide)	5.20	Asp199	H bond	O-H	2.21
	π - π stacked						
Tyr63	π - π <i>T</i> -shaped	Benzene (Ring B)	4.50	Asp326	H bond	O-H	2.86
Tyr63	π -alkyl/ Alkyl	Cl	5.14	Asp382	H bond	O-H	2.38
His103	π -alkyl/ Alkyl	Cl	4.60		Carbon H bond	C-O	2.88
Ala200	π -alkyl/ Alkyl	Cl	3.45		H bond	O-H	2.27
Arg381	π -alkyl/ Alkyl	Benzene (Phenyl sulfonamide)	5.02	Ala59	Carbon H bond	C-O	3.42
Asp382	π -cation/anion	Benzene (Ring A)	3.58	Asn258	Carbon H bond	C-O	3.74
Arg415	π -cation/anion	Benzene (Ring A)	4.18	Asp60	Carbon H bond	C-O	3.45
				Tyr63	π -sigma	C-O	3.97
				Phe144	π -alkyl	CH ₃	4.95
				Phe163	π -alkyl	CH ₃	4.40

protein was generated by the MODELER protocol and the optimized structure was further validated by the Ramachandran plot (see [Supporting Information](#)) obtained from RAMPAGE server. According to the Ramachandran plot, 95.3% of residues were found in the favored regions while 4.7% of residues were in the allowed regions. In addition, with no detection of outlier residues, the generated homology model was therefore deemed acceptable.

Based on the molecular docking analysis (Fig. 8A), the sulfonamide moiety of compound **18** forms two strong hydrogen bonding (green dashed line) interactions with Tyr15 and Asn58 residues. Meanwhile, the phenyl moiety of Ring A was found to bond with Asp382 and Arg415 residues, through the additional π -cation/anion (orange dashed line) interactions, respectively. These findings, therefore, justify the important role of the extended sulfonamide-containing Ring A in

enhancing the α -glucosidase inhibition property. On the other hand, the *p*-chloro group of the Ring B fragment displayed hydrophobic contact (light purple dashed line) with Tyr63, His103, and Ala200 residues on the active site. This observation could be used to explain the better performance of chlorinated compounds compared to their respective non-chlorinated analogues. Meanwhile, interaction mode of acarbose with the homology modeled bacterial α -glucosidase protein revealed several hydrogen-bonding interactions with the protein residues (Ala200, Asn324, Arg415, Asp199, Asp326, Asp382 and Ala59) in the active site of α -glucosidase (Fig. 8B), thereby justifying the higher α -glucosidase inhibitory potency than **18**. All the binding interactions involved were tabulated in Table 2.

Compound **1** – **17** were also docked individually into the same active pocket site of homology bacterial α -glucosidase model to rationally

Table 3
Data of selected interactions resulting from the molecular docking of compounds 1–17 into α -glucosidase.

Compounds	IC ₅₀ (μ M)	Protein-ligand interactions			
		Ligand	Receptors	Interaction	Bonding distance (Å)
1	ND	C=O	Arg415	H bond	2.45
2	ND	C=O	Arg415	H bond	2.46
3	ND	–	–	–	–
4	ND	–NH	Asp382	H bond	2.00
5	ND	C of –OCH ₃	Glu256	Carbon H bond	3.34
6	ND	C=O	His103	H bond	2.70
		C=O	Gln167	H bond	2.04
		N–H	Glu256	H bond	2.07
7	ND	N–H	Asp382	H bond	2.04
8	ND	N–H	Asn58	H bond	2.00
		N–H	Asn58	H bond	2.65
9	ND	N–H	Asp382	H bond	2.34
		N–H	Asp382	H bond	2.66
10	6.29 \pm 0.9	S=O	Arg415	H bond	1.98
		S=O	Asn61	H bond	3.06
		F of –CF ₃	Trp434	π -alkyl/ Alkyl	4.90
11	7.16 \pm 0.5	F of –CF ₃	Gln167	H bond	2.65
		N–H	Asn258	H bond	2.69
12	8.63 \pm 4.4	S=O	Arg415	H bond	2.49
		S=O	Arg415	H bond	2.73
		F of –CF ₃	Trp434	π -alkyl/ Alkyl	5.19
13	14.04 \pm 1.2	N–H	Asn258	H bond	2.20
		F of –CF ₃	Gln167	Halogen (F)	3.18
		F of –CF ₃	Gln167	Halogen (F)	3.16
14	11.69 \pm 0.9	F of –CF ₃	Gln167	H bond	2.49
		S=O	Arg197	H bond	2.80
		N–H	Asp326	H bond	2.35
		F of –CF ₃	Asp60	Halogen (F)	3.43
		F of –CF ₃	Glu256	π -anion	4.91
15	12.16 \pm 2.1	S=O	Tyr15	H bond	2.92
		S=O	Arg415	H bond	2.52
		C of –OCH ₃	Glu256	Carbon H bond	3.61
		N–H	Asn258	H bond	2.07
		F of –CF ₃	Gln167	Halogen (F)	3.16
17	7.21 \pm 0.4	F of –CF ₃	Gln167	Halogen (F)	3.19
		F of –CF ₃	Gln167	H bond	2.49
		S=O	Arg197	H bond	2.80
		N–H	Asp326	H bond	2.46
		F of –CF ₃	Asp60	Halogen (F)	3.23

explore their chemical space in the active sites and thus establish the SAR. Based on the results, it is conceivable that the multiple H-bonds generated through the N, O and/or F atoms of trifluoromethylbenzene sulfonamide moiety in coupled with the halogen (fluorine) bonds to the active site residues as observed in the sulfonamide-containing analogues (10–17) might contribute to the enhanced α -glucosidase inhibitory properties. On the contrary, the H-bonds formed through –NH and C=O groups are less significant to influence the α -glucosidase inhibition potency as exerted by 1–9, thus verifying the importance of the trifluoromethylbenzene sulfonamide sub-structure of the molecules. The selected binding interactions of 1–17 were summarized in Table 3, while the docking illustrations were compiled in Supporting Information.

Additionally, compound 18 was docked on the human lysosomal acid α -glucosidase (GAA, PDB ID: 5NN8) active site to predict its binding mechanism on the human α -glucosidase enzyme (Fig. 9A). The catalytic site of human GAA is mainly composed of acidic (Asp404, Asp518, Glu521 and Asp616) and basic residues (Arg600 and His674) [59]. The structure of human α -glucosidase is resembling the structures of human glucoside hydrolase family, GH311 homologues, maltase glucoamylase and sucrase-isomaltase. The N-terminal trefoil type-P

domain is linked to a domain composed of β -sheet, catalytic (β/α)8 barrel made of two inserts β 3 (insert I) and β 4 (insert II), as well as the proximal and distal β -sheet domains located at the C-terminus. The substrate-binding pocket is narrow and positioned near the C-terminal ends of β -strands of the catalytic (β/α)8 domain and was shaped by a loop from the N-terminal β -sheet domain and both inserts I and II. The Asp518 and Asp616 residues were determined to act as the catalytic nucleophile and catalytic acid/base, respectively [59].

Results showed that 18 binds with His674 and Asp616 via H-bonds and the acidic residues (Asp404, Asp518 and Asp616) on the active site by halogen (fluorine) and π -anion interactions. Moreover, Trp481, Trp516, Phe649 and His674 interacts hydrophobically to the trifluoromethylbenzene sulfonamide moiety, in which further confirming the critical role of the extended sulfonamide-containing Ring A fragment in eliciting the α -glucosidase inhibitor potency of 18. For comparison, the standard drug acarbose was docked into the same active site of this crystal. The multiple numbers of H-bonds formed between acarbose with the Asp518, Asp616 and Arg600 residues of the GAA active site, thus suggested a higher α -glucosidase inhibition activity compared to 18. The binding interaction of compounds 18 and acarbose in the active site of human GAA are shown in Table 4.

Considering a multiple interactions between 18 and important residues in the active sites of human α -glucosidase, this bioactive analogue 18 deserved further biological investigation with regards of its potency on the expression of multiple human α -glucosidases including lysosomal GAA, ER-localised GANAB and intestinal maltase-glucoamylase (MGAM) towards the development of promising drug candidates for the treatment of T2DM.

Our study also focused on understanding the binding mode of diarylpentadienone moiety, and to investigate the necessary interactions required for DPP-4 inhibition. With the collected *in vitro* results in hand, the most active compound 15 was further subjected to a molecular docking study to explicate key molecular interactions. To begin, the protein structure of DPP-4 (PDB ID: 5T4B) was retrieved from the Brookhaven Protein Data Bank (PDB).

The DPP-4 enzyme consists of two domains, an eight-stranded β -propeller domain at the N-terminus and an α/β -hydrolase domain at the C-terminus. The X-ray crystal study of various inhibitors in complex with DPP-4 revealed that the binding site of DPP-4 mainly comprises of three parts: an S1 pocket, the N-terminal recognition region, and an S2 pocket. The S1 hydrophobic pocket consisted of residues Tyr631, Val656, Trp659, Tyr662, Tyr666, and Val711 adjacent to the catalytic triad of the active site. The active site is positioned in the hydrolase domain and comprised of catalytic triad residues Ser630, Asp708, and His740. The N-terminal recognition region is formed by Glu205, Glu206, and Tyr662, while the hydrophobic S2 pocket, which is larger compared with S1, is surrounded by residues Phe357, Arg358, Ser209, and Tyr666.

Fig. 10 illustrates the molecular interactions of compound 15 with DPP-4. It has been found that the oxygen of the carbonyl group present on the bridge of the diarylpentadienone forms a carbon-hydrogen bond with Ser630, a vital residue for the N-terminal recognition site. The secondary amino group present on Ring A protrudes towards the Ser630 and Tyr631 of the S1 pocket by creating a hydrogen bond with the neighboring Tyr547. All other interactions are tabulated in Table 5.

2.7. Conclusion

In conclusion, a new series of non-PAINS associated diarylpentadienone derivatives (1–18) were successfully synthesized and have shown their potential as effective and selective anti-diabetic promising molecules against α -glucosidase through *in vitro* experimental evidence. The significance of *p*-sulfonamide-diarylpentadienones with halogenated (-Cl) phenyl (Ring B) of compound 18 was demonstrated to possess remarkable α -glucosidase inhibition activities with an IC₅₀ value of 5.69 \pm 0.7 μ M through competitive mode. Furthermore,

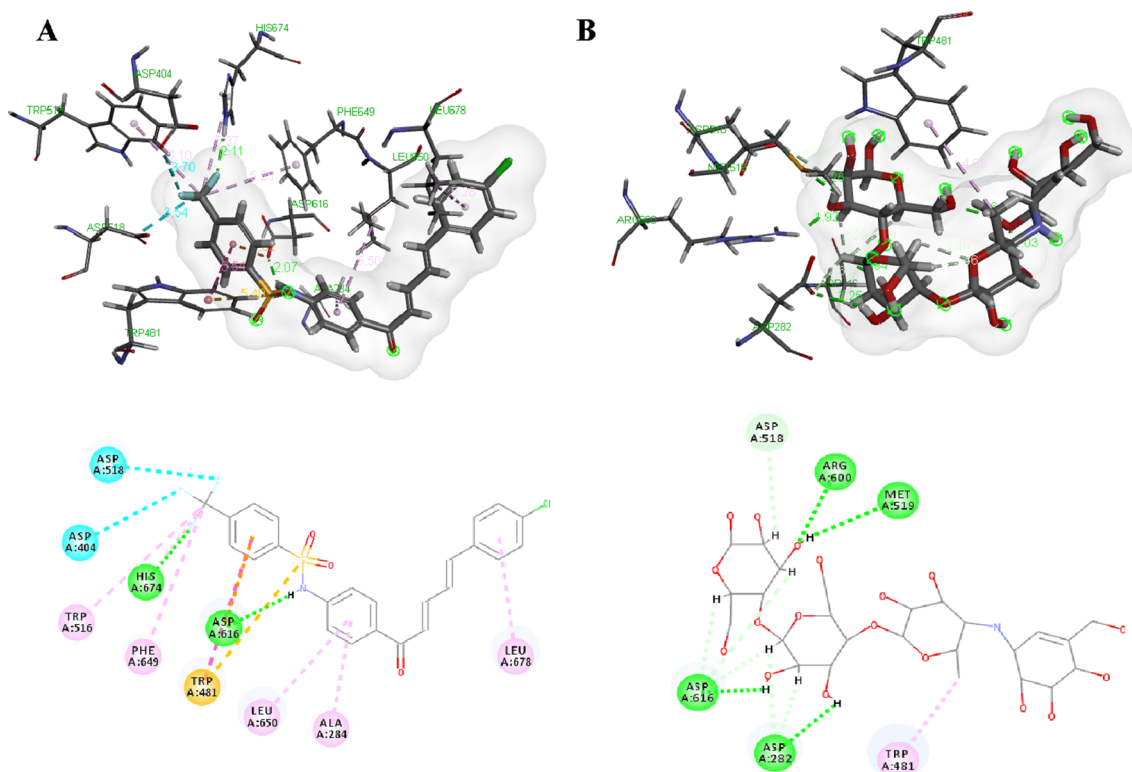


Fig. 9. 3D and 2D diagram of the binding interactions of (A) compound **18** and (B) acarbose on the human lysosomal α -glucosidase receptor. (Green line: H bond; orange line: π -cation/anion; purple line: π - π stacked/*T*-shaped; light purple: Alkyl/ π -Alkyl; cyan line: Halogen (Fluorine); yellow line: π -Sulfur). (For interpretation of the references to colour in this figure legend, the reader is referred to the web version of this article.)

compound **18** recorded no signs of toxicity, particularly on the normal embryonic development, blood vessel formation and apoptosis of zebrafish *in vivo* model. Overall, these results suggest that compound **18** could be a promising candidate towards the discovery of a new anti-diabetic agent and can serve as a basis for further studies involving the *in vivo* efficacy and safety assessment in the animal models.

3. Experimental section

3.1. PAINS and aggregator filtration

3.1.1. *In-silico* PAINS identification

All chemical structures of the diarylpentadienones series and its derivatives were drawn using ChemDraw Ultra 12.0 and subsequently

converted to SMILES (Simplified Molecular Input Line Entry System) format. The SMILES formulas were then converted into Symyx SDF (Spatial Data File) file format as recommended by the FAF-Drugs4 Bank Formatter (<http://mobylye.rpbs.univ-paris-diderot.fr/cgi-bin/portal.py#forms::Bank-Formatter>), before automatically redirected as the input file into the FAF-Drugs4 server (<http://mobylye.rpbs.univ-paris-diderot.fr/cgi-bin/portal.py#forms::FAF-Drugs4>) for the filtration of PAINS using PAINS filter A, B, and C [42]. The generated results are available at the following address (http://mobylye.rpbs.univ-paris-diderot.fr/cgi-bin/portal.py?form=admetox#jobs::FAF-Drugs4_T05472492539883).

3.1.2. *In-silico* aggregator identification

The SMILES file containing the synthesized molecules generated

Table 4

Data of interactions resulting from the molecular docking of compounds **18** and acarbose into human lysosomal α -glucosidase.

Compound 18				Acarbose			
Active site	Interactions	With	Bonding distance (Å)	Active site	Interactions	With	Bonding distance (Å)
His674	H bond	F	2.11	Arg600	H Bond	O–H	1.92
Asp616	H bond	N–H	2.07	Met519	H Bond	O–H	2.26
Asp404	Halogen (fluorine)	F	3.70	Asp282	H Bond	O–H	2.25
Asp518	Halogen (fluorine)	F	3.54		Carbon H Bond	C–H	2.61
Asp616	π -anion	Benzene (Phenyl sulfonamide)	3.82		Carbon H Bond	C–H	2.71
Trp481	π -sulfur	S	5.40	Asp616	H Bond	O–H	1.94
Trp481	π - π <i>T</i> -shaped	Benzene (Phenyl sulfonamide)	5.53		Carbon H Bond	C–H	3.10
Trp516	π -alkyl	CF ₃	5.10		Carbon H Bond	C–H	2.62
Phe649	π -alkyl	CF ₃	5.25	Asp518	Carbon H Bond	C–H	2.70
His674	π -alkyl	CF ₃	5.37	Asp616	Carbon H Bond	C–H	2.29
Ala284	π -alkyl	Benzene (Ring A)	5.08	Trp481	π -alkyl	CH ₃	4.40
Leu650	π -alkyl	Benzene (Ring A)	5.50				
Leu678	π -alkyl	Benzene (Ring B)	5.28				

acetone- d_6): δ = 113.0, 113.1, 125.9, 126.9, 127.0 (2 \times Ar-CH), 127.6, 128.7, 128.8 (2 \times Ar-CH), 130.6 (2 \times Ar-CH), 136.6, 139.8, 141.8, 153.3, 186.2; HRMS (ESI): m/z calcd for $C_{17}H_{15}ON\cdot H$: 248.0790 [M-H]⁻; found: 248.0788.

3.3.4. 1-(2-Aminophenyl)-5-(4-methoxyphenyl)penta-2,4-dien-1-one (4)

Yellow solid; 10% crude; mp 95–96°C; IR (UATR) 3297 (NH, str.), 2918 (sp³ CH, str.) 1538 (C=O, str.), 1349 (C=C, str.) cm⁻¹; ¹H NMR (500 MHz, CDCl₃): δ = 3.84 (s, 3H, CH₃), 6.30 (s, 2H, NH₂), 6.67 (d, J = 7.1 Hz, 1H, Ar-CH), 6.68 (d, J = 8.4 Hz, 1H, Ar-CH), 6.91 (td, J = 9.2, 1.7 Hz, 1H, Ar-CH), 6.91 (d, J = 15.3 Hz, 1H, CH = CH-Ar), 6.92 (d, J = 8.9 Hz, 1H, Ar-CH), 6.93 (app. t, J = 15.3 Hz, 1H, CH = CH-Ar), 7.14 (d, J = 14.7 Hz, 1H, COCH = CH), 7.28 (d, J = 7.4 Hz, 1H, Ar-CH), 7.44 (d, J = 8.6 Hz, 2H, 2 \times Ar-CH), 7.53 (dd, J = 14.7, 9.4 Hz, 1H, COCH = CH), 7.79 (d, J = 8.0 Hz, 1H, Ar-CH); ¹³C NMR (126 MHz, CDCl₃): δ = 55.2, 114.2 (2 \times Ar-CH), 115.8, 117.2, 119.2, 125.1, 125.3, 128.6 (2 \times Ar-CH), 129.1, 130.8, 134.0, 140.6, 143.6, 150.8, 160.3, 191.8; HRMS (ESI): m/z calcd for $C_{18}H_{17}NO_2\cdot H$: 278.0800 [M-H]⁻; found: 278.0788.

3.3.5. 1-(3-Aminophenyl)-5-(4-methoxyphenyl)penta-2,4-dien-1-one (5)

Orange solid; 23% crude; mp 151–152°C; IR (UATR) 3448, 3352 (NH, str.), 2925 (sp³ CH, str.) 1562 (C=O, str.), 1448 (C=C, str.) cm⁻¹; ¹H NMR (500 MHz, acetone- d_6): δ = 3.91 (s, 3H, CH₃), 4.98 (s, 2H, NH₂), 6.98 (d, J = 7.8 Hz, 1H, Ar-CH), 7.04 (d, J = 8.6 Hz, 2H, 2 \times Ar-CH), 7.17 (d, J = 6.6 Hz, 1H, Ar-CH), 7.24 (d, J = 14.8 Hz, 1H, COCH = CH), 7.28 (d, J = 16.5 Hz, 1H, CH = CH-Ar), 7.31 (dd, J = 16.5, 10.3 Hz, 1H, CH = CH-Ar), 7.38 (s, 1H, Ar-CH), 7.59 (dd, J = 14.8, 10.3 Hz, 1H, COCH = CH), 7.64 (d, J = 8.6 Hz, 2H, 2 \times Ar-CH); ¹³C NMR (126 MHz, acetone- d_6): δ = 55.0, 113.5, 114.5 (2 \times Ar-CH), 116.8, 118.6, 124.8, 125.3 (2 \times Ar-CH), 128.9, 129.3, 129.4, 139.6, 141.2, 144.3, 148.9, 160.9, 189.5; HRMS (ESI): m/z calcd for $C_{18}H_{17}NO_2\cdot H$: 278.0800 [M-H]⁻; found: 278.0808.

3.3.6. 1-(4-Aminophenyl)-5-(4-methoxyphenyl)penta-2,4-dien-1-one (6)

Yellow solid; 40% crude; mp 98–99°C; IR (UATR) 3331, 3206 (NH, str.), 2921 (sp³ CH, str.) 1561 (C=O, str.), 1256 (C=C, str.) cm⁻¹; ¹H NMR (500 MHz, acetone- d_6): δ = 3.83 (s, 3H, CH₃), 5.53 (s, 2H, NH₂), 6.73 (d, J = 8.4 Hz, 2H, 2 \times Ar-CH), 6.96 (d, J = 8.5 Hz, 2H, 2 \times Ar-CH), 7.06 (d, J = 14.6 Hz, 1H, COCH = CH), 7.07 (dd, J = 15.6, 9.5 Hz, 1H, CH = CH-Ar), 7.26 (d, J = 15.6 Hz, 1H, CH = CH-Ar), 7.49 (dd, J = 14.6, 9.5 Hz, 1H, COCH = CH), 7.54 (d, J = 8.5 Hz, 2H, 2 \times Ar-CH), 7.86 (d, J = 8.4 Hz, 2H, 2 \times Ar-CH); ¹³C NMR (126 MHz, acetone- d_6): δ = 54.7, 113.1 (2 \times Ar-CH), 114.2 (2 \times Ar-CH), 124.6, 125.3, 127.0, 128.5 (2 \times Ar-CH), 129.3, 130.5 (2 \times Ar-CH), 139.8, 142.4, 153.2, 160.4, 186.2; HRMS (ESI): m/z calcd for $C_{18}H_{17}NO_2\cdot H$: 278.0800 [M-H]⁻; found: 278.0785.

3.3.7. 1-(2-Aminophenyl)-5-(4-chlorophenyl)penta-2,4-dien-1-one (7)

Yellow solid; 28% crude; mp 109–110°C; IR (UATR) 3302 (NH, str.), 1617 (C=C, str.) 1564 (C=O, str.), cm⁻¹; ¹H NMR (500 MHz, acetone- d_6): δ = 6.61 (t, 1H, Ar-CH), 6.83 (d, J = 8.3 Hz, 1H, Ar-CH), 7.11 (s, 2H, NH₂), 7.11 (d, J = 15.6 Hz, 1H, CH = CH-Ar), 7.27 (app. t, J = 6.8 Hz, 1H, Ar-CH), 7.27 (dd, J = 15.6, 10.5 Hz, 1H, CH = CH-Ar), 7.43 (d, J = 8.5 Hz, 2H, 2 \times Ar-CH), 7.47 (d, J = 14.7 Hz, 1H, COCH = CH), 7.50 (dd, J = 14.7, 10.5 Hz, 1H, COCH = CH), 7.63 (dd, J = 1.00 Hz, 2H, 2 \times Ar-CH), 7.88 (d, J = 8.1 Hz, 1H, Ar-CH); ¹³C NMR (126 MHz, acetone- d_6): δ = 114.7, 117.0, 118.2, 127.3, 128.3, 128.5 (2 \times Ar-CH), 128.9 (2 \times Ar-CH), 130.7, 133.8, 134.0, 135.5, 138.4, 141.9, 152.1, 190.6; HRMS (ESI): m/z calcd for $C_{17}H_{14}ClNO\cdot H$: 282.0610 [M-H]⁻; found: 282.0607.

3.3.8. 1-(3-Aminophenyl)-5-(4-chlorophenyl)penta-2,4-dien-1-one (8)

Yellow solid; 31% crude; mp 132–133°C; IR (UATR) 3350 (NH, str.), 1564 (C=O, str.), 1488 (C=C, str.) cm⁻¹; ¹H NMR (500 MHz, acetone- d_6): δ = 4.92 (s, 2H, NH₂), 6.92 (ddd, J = 7.8, 2.3, 1.0 Hz, 1H, Ar-

CH), 7.18 (d, J = 15.8 Hz, 1H, CH = CH-Ar), 7.23 (d, 15.0, 1H, COCH = CH), 7.23 (app. d, 1H), 7.24 (dd, 15.8, 10.8, CH = CH-Ar), 7.25 (d, J = 5.5, 1H, Ar-CH), 7.31 (s, 1H, Ar-CH), 7.44 (d, J = 8.5 Hz, 2H, 2 \times Ar-CH), 7.54 (dd, J = 15.0, 10.8 Hz, 1H, COCH = CH), 7.63 (d, J = 8.5 Hz, 2H, 2 \times Ar-CH); ¹³C NMR (126 MHz, acetone- d_6): δ = 113.3, 116.7, 118.6, 126.4, 128.1, 128.7 (2 \times Ar-CH), 128.9 (2 \times Ar-CH), 129.1, 134.0, 135.3, 139.1, 139.4, 143.2, 148.9, 189.4; HRMS (ESI): m/z calcd for $C_{17}H_{14}ClNO\cdot H$: 282.0610 [M-H]⁻; found: 282.0613.

3.3.9. 1-(4-Aminophenyl)-5-(4-chlorophenyl)penta-2,4-dien-1-one (9)

Yellow solid; 12% crude; mp 145–146°C; IR (UATR) 3352 (NH, str.), 1571 (C=O, str.), 1260 (C=C, str.) cm⁻¹; ¹H NMR (500 MHz, acetone- d_6): δ = 5.53 (d, J = 7.2 Hz, 2H, NH₂), 6.73 (d, J = 8.4 Hz, 2H, 2 \times Ar-H), 7.15 (d, J = 15.6 Hz, 1H, CH = CH-Ar), 7.30 (dd, J = 15.6, 11.0 Hz, 1H, CH = CH-Ar), 7.40 (d, J = 14.8 Hz, 1H, COCH = CH), 7.49 (d, J = 8.3 Hz, 2H, 2 \times Ar-H), 7.54 (dd, J = 14.8, 11.0 Hz, 1H, COCH = CH), 7.68 (d, J = 8.3 Hz, 2H, 2 \times Ar-H), 7.92 (d, J = 8.4 Hz, 2H, 2 \times Ar-H); ¹³C NMR (126 MHz, acetone- d_6): δ = 113.1, 113.2, 126.5, 128.3, 128.5, 128.6 (2 \times Ar-CH), 128.9 (2 \times Ar-CH), 130.7 (2 \times Ar-CH), 133.8, 135.6, 138.2, 141.5, 145.7, 186.2; HRMS (ESI): m/z calcd for $C_{17}H_{14}ClNO\cdot H$: 282.0610 [M-H]⁻; found: 282.0606.

3.4. General procedure for the synthesis of sulfonylated-diarylpentadienone (10–18)

The sulfonamide-containing diarylpentadienones (10–18) were synthesized via condensation of equimolar quantity of 4-trifluoromethylbenzenesulfonyl chloride and aminated-diarylpentadienone (1–9) in methanol (5 ml) prior to the addition of pyridine as a catalyst (3–5 drops) once the homogenous mixture was obtained. The reaction mixture was left to stir for 24 h at room temperature and monitored with TLC to complete reaction. Ten mL of water was then poured to the reaction mixture to quench the reaction and the solid products were collected, while extraction with ethyl acetate was carried out for the non-precipitated mixture. The obtained products were combined and subjected to column chromatography before further recrystallization to yield a purified end-product.

3.4.1. N-[2-(5-phenylpenta-2,4-dienoyl)phenyl]-4-trifluoromethylbenzenesulfonamide (10)

Pale yellow solid; 8% crude; mp 105–106°C; IR (UATR) 1622 (C=O, str.), 1560 (C=C, str.), 1230 (S=O, assym.), 1144 (S=O, symm.) cm⁻¹; ¹H NMR (500 MHz, CDCl₃): δ = 6.90 (d, J = 15.0 Hz, 1H, COCH = CH), 6.96 (dd, J = 15.5, 10.6 Hz, 1H, CH = CH-Ar), 7.06 (d, J = 15.5 Hz, 1H, CH = CH-Ar), 7.17 (t, J = 7.6 Hz, 1H, Ar-CH), 7.38 (dd, J = 15.0, 10.6 Hz, 1H, COCH = CH), 7.39 (d, J = 7.4 Hz, 2H, 2 \times Ar-CH), 7.50 (t, J = 7.4 Hz, 1H), 7.52 (app. m, 3H), 7.66 (d, J = 8.1 Hz, 2H, 2 \times Ar-CH), 7.74 (d, J = 8.2 Hz, 1H, Ar-CH), 7.80 (d, J = 7.8 Hz, 1H, Ar-CH), 7.92 (d, J = 8.1 Hz, 2H, 2 \times Ar-CH), 11.38 (s, 1H, NH); ¹³C NMR (126 MHz, acetone- d_6): δ = 118.6, 120.3, 123.4, 123.9, 124.8, 125.3, 126.8, 127.4 (2 \times Ar-CH), 128.0 (2 \times Ar-CH), 128.1, 128.9 (2 \times Ar-CH), 129.4, 131.1, 132.8, 134.5, 135.0, 136.2, 139.2, 143.1, 146.4, 192.9; HRMS (ESI): m/z calcd for $C_{24}H_{18}F_3NO_3S\cdot H$: 456.0190 [M-H]⁻; found: 456.0188.

3.4.2. N-[3-(5-phenylpenta-2,4-dienoyl)phenyl]-4-trifluoromethylbenzenesulfonamide (11)

Pale yellow solid; 22% crude; mp 145–146°C; IR (UATR) 3358 (NH, str.), 1572 (C=O, str.), 1275 (C=C, str.), 1145 (S=O, assym.), 998 (S=O, symm.) cm⁻¹; ¹H NMR (500 MHz, acetone- d_6): δ = 7.19 (d, J = 15.5 Hz, 1H, CH = CH-Ar), 7.22 (d, J = 14.5 Hz, 1H, COCH = CH), 7.25 (dd, J = 15.5, 10.2 Hz, 1H, CH = CH-Ar), 7.36 (t, J = 7.3 Hz, 1H, Ar-CH), 7.41 (d, J = 7.7 Hz, 1H, Ar-CH), 7.42 (d, J = 7.1 Hz, 1H, Ar-CH), 7.47 (d, J = 6.9 Hz, 1H, Ar-CH), 7.48 (app. t, J = 8.0, 1H, Ar-CH), 7.56 (dd, J = 14.9, 10.2 Hz, 1H, COCH = CH),

7.62 (d, $J = 7.4$ Hz, 2H, 2 × Ar-CH), 7.79 (dt, $J = 6.5, 1.8$ Hz, 1H, Ar-CH), 7.88 (d, $J = 2.0$ Hz, 1H, Ar-CH), 7.93 (d, $J = 8.4$ Hz, 2H, 2 × Ar-CH), 8.06 (d, $J = 8.3$ Hz, 2H, 2 × Ar-CH); ^{13}C NMR (126 MHz, acetone- d_6): $\delta = 120.4, 124.7, 124.9, 125.0, 126.3, 126.4, 127.1, 127.3$ (2 × Ar-CH), 127.9 (2 × Ar-CH), 128.8 (2 × Ar-CH), 129.2, 129.7, 133.5, 133.8, 136.3, 137.8, 139.3, 141.9, 143.5, 144.7, 188.3; HRMS (ESI): m/z calcd for $\text{C}_{24}\text{H}_{18}\text{F}_3\text{NO}_3\text{S}\text{-H}^+$: 456.1020 [M-H] $^+$; found: 456.1022.

3.4.3. *N*-[4-(5-phenylpenta-2,4-dienoyl)phenyl]-4-trifluoromethylbenzenesulfonamide (12)

Pale yellow solid; 27% crude; mp 178-179°C; IR (UATR) 3041 (NH, str.), 1578 (C=O, str.), 1306 (C=C, str.), 1136 (S=O, assym.), 1010 (S=O, symm.) cm^{-1} ; ^1H NMR (500 MHz, acetone- d_6): $\delta = 7.17$ (d, $J = 15.6$ Hz, 1H, CH = CH-Ar), 7.22 (app. dd, $J = 10.2$ Hz, 1H), 7.30 (d, $J = 14.8$ Hz, 1H, COCH = CH), 7.36 (d, $J = 7.2$ Hz, 1H, Ar-CH), 7.40 (d, $J = 6.6$ Hz, 2H, 2 × Ar-CH), 7.41 (dd, $J = 15.6, 10.2$ Hz, 1H, CH = CH-Ar), 7.55 (dd, $J = 14.8, 10.2$ Hz, 1H, COCH = CH), 7.61 (d, $J = 7.4$ Hz, 2H, 2 × Ar-CH), 7.95 (d, $J = 8.4$ Hz, 2H, 2 × Ar-CH), 7.99 (d, $J = 8.7$ Hz, 2H, 2 × Ar-CH), 8.12 (d, $J = 8.3$ Hz, 2H, 2 × Ar-CH); ^{13}C NMR (126 MHz, acetone- d_6): $\delta = 119.3, 125.2, 126.5, 126.6, 127.2, 127.3$ (2 × Ar-CH), 128.1 (2 × Ar-CH), 128.9 (2 × Ar-CH), 129.2, 129.9 (2 × Ar-CH), 132.6, 134.3, 136.5, 141.5, 141.6, 144.1, 187.5; HRMS (ESI): m/z calcd for $\text{C}_{24}\text{H}_{18}\text{F}_3\text{NO}_3\text{S}\text{-H}^+$: 456.0550 [M-H] $^+$; found: 456.0555.

3.4.4. *N*-(2-[5-(4-methoxyphenyl)penta-2,4-dienoyl]phenyl)-4-trifluoromethylbenzenesulfonamide (13)

Pale yellow solid; 11% crude; mp 178-179°C; IR (UATR) 3325 (NH, str.), 2932 (CH alkane, str.), 1543 (C=O, str.), 1309 (C=C, str.), 1270 (S=O, assym.), 1144 (S=O, symm.) cm^{-1} ; ^1H NMR (500 MHz, acetone- d_6): $\delta = 3.83$ (s, 3H, CH_3), 6.99 (d, $J = 8.8$ Hz, 2H, 2 × Ar-CH), 7.08 (dd, $J = 15.5, 11.0$ Hz, 1H, CH = CH-Ar), 7.17 (d, $J = 14.7$ Hz, 1H, COCH = CH), 7.21 (d, $J = 15.5$ Hz, 1H, CH = CH-Ar), 7.59 (d, $J = 8.8$ Hz, 1H, 2 × Ar-CH), 7.60 (dd, $J = 14.7, 11.0$ Hz, 1H, COCH = CH), 7.60 (app. t, $J = 8.1$ Hz, 1H, Ar-CH), 7.72 (d, $J = 7.7$ Hz, 1H, Ar-CH), 7.89 (d, $J = 8.4$ Hz, 2H, 2 × Ar-CH), 8.03 (d, $J = 7.7$ Hz, 1H, Ar-CH), 8.04 (d, $J = 8.1$ Hz, 2H, 2 × Ar-CH), 11.67 (s, 1H, NH); ^{13}C NMR (126 MHz, acetone- d_6): $\delta = 54.8, 114.3$ (2 × Ar-CH), 120.3, 123.9, 124.0, 124.6, 126.4, 128.1 (2 × Ar-CH), 128.9, 129.1 (2 × Ar-CH), 131.0, 134.4, 143.3, 147.1, 161.1, 192.8, 205.6; HRMS (ESI): m/z calcd for $\text{C}_{25}\text{H}_{20}\text{F}_3\text{NO}_4\text{S}\text{-H}^+$: 486.0880 [M-H] $^+$; found: 486.0878.

3.4.5. *N*-(3-[5-(4-methoxyphenyl)penta-2,4-dienoyl]phenyl)-4-trifluoromethylbenzenesulfonamide (14)

Pale yellow solid; 23% crude; mp 178-179°C; IR (UATR) 3300 (NH, str.), 2924 (CH alkane, str.), 1561 (C=O, str.), 1319 (C=C, str.), 1239 (S=O, assym.), 1152 (S=O, symm.) cm^{-1} ; ^1H NMR (500 MHz, acetone- d_6): $\delta = 3.84$ (s, 3H, CH_3), 6.98 (d, $J = 8.7$ Hz, 2H, 2 × Ar-CH), 7.09 (dd, $J = 15.7, 10.0$ Hz, 1H, CH = CH-Ar), 7.13 (d, $J = 14.6, 10.0$ Hz, 1H, COCH = CH), 7.15 (d, $J = 15.7$ Hz, 1H, CH = CH-Ar), 7.45 (app. d, $J = 8.0$ Hz, 1H, Ar-CH), 7.46 (d, $J = 5.5$ Hz, Ar-CH), 7.55 (dd, $J = 14.6, 10.0$ Hz, 1H, COCH = CH), 7.58 (d, $J = 8.7$ Hz, 1H, 2 × Ar-CH), 7.78 (dd, $J = 8.0, 2.0$ Hz, 1H, Ar-CH), 7.86 (s, 1H, Ar-CH), 7.93 (d, $J = 8.3$ Hz, 2H, 2 × Ar-CH), 8.05 (d, $J = 8.3$ Hz, 2H, 2 × Ar-CH), 9.50 (s, 1H, NH); ^{13}C NMR (126 MHz, acetone- d_6): $\delta = 54.9, 114.4$ (2 × Ar-CH), 120.5, 123.8, 124.8, 124.9, 125.0, 126.5, 126.5, 128.1 (2 × Ar-CH), 129.0 (2 × Ar-CH), 129.1, 129.8, 131.0, 131.1, 133.4, 135.8, 139.6, 142.1, 145.5, 160.9, 188.3; HRMS (ESI): m/z calcd for $\text{C}_{25}\text{H}_{20}\text{F}_3\text{NO}_4\text{S}\text{-H}^+$: 486.1590 [M-H] $^+$; found: 486.1588.

3.4.6. *N*-(4-[5-(4-methoxyphenyl)penta-2,4-dienoyl]phenyl)-4-trifluoromethylbenzenesulfonamide (15)

Pale yellow solid; 34% crude; mp 178-179°C; IR (UATR) 3148 (NH, str.), 2925 (CH alkane, str.), 1587 (C=O, str.), 1508 (C=C, str.), 1316

(S=O, assym.), 1153 (S=O, symm.) cm^{-1} ; ^1H NMR (500 MHz, acetone- d_6): $\delta = 3.84$ (s, 3H, CH_3), 6.97 (d, $J = 8.7$ Hz, 2H, 2 × Ar-CH), 7.01 (d, $J = 15.5$ Hz, 1H, CH = CH-Ar), 7.11 (dd, $J = 15.5, 10.0$ Hz, 1H, CH = CH-Ar), 7.22 (d, $J = 14.8$ Hz, 1H, COCH = CH), 7.39 (d, $J = 8.6$ Hz, 2H, 2 × Ar-CH), 7.40 (dd, $J = 8.7, 3.2$ Hz, 1H, Ar-H), 7.54 (dd, $J = 14.8, 10.0$ Hz, 1H, COCH = CH), 7.56 (d, $J = 8.7$ Hz, 2H, 2 × Ar-CH), 7.94 (s, 1H, Ar-CH), 7.97 (d, $J = 8.7$ Hz, 2H, 2 × Ar-CH), 8.12 (d, $J = 8.4$ Hz, 2H, 2 × Ar-CH); ^{13}C NMR (126 MHz, acetone- d_6): $\delta = 54.95, 114.4$ (2 × Ar-CH), 118.9 (2 × Ar-CH), 126.3, 126.4, 126.4, 126.5, 126.5, 127.0 (2 × Ar-CH), 127.9, 129.7 (2 × Ar-CH), 130.4 (2 × Ar-CH), 133.2, 141.6, 143.5, 152.4, 162.2, 193.0; HRMS (ESI): m/z calcd for $\text{C}_{25}\text{H}_{20}\text{F}_3\text{NO}_4\text{S}\text{-H}^+$: 486.1720 [M-H] $^+$; found: 486.1716.

3.4.7. *N*-(2-[5-(4-chlorophenyl)penta-2,4-dienoyl]phenyl)-4-trifluoromethylbenzenesulfonamide (16)

Pale yellow solid; 38% crude; mp 178-179°C; IR (UATR) 3093 (NH, str.), 1567 (C=O, str.), 1489 (C=C, str.), 1319 (S=O, assym.), 1157 (S=O, symm.) cm^{-1} ; ^1H NMR (500 MHz, acetone- d_6): $\delta = 7.22$ (dd, $J = 15.5, 7.4$ Hz, 1H, CH = CH-Ar), 7.25 (app. m, 2H) 7.26 (d, $J = 15.2$ Hz, 1H, CH = CH-Ar), 7.27 (d, $J = 15.5$ Hz, 1H, CH = CH-Ar), 7.27 (d, $J = 14.7$ Hz, 1H, COCH = CH), 7.46 (d, $J = 8.5$ Hz, 2H, 2 × Ar-CH), 7.56 (dd, $J = 14.7, 7.4$ Hz, 1H, COCH = CH), 7.61 (d, $J = 8.3$ Hz, 1H, Ar-CH), 7.65 (d, $J = 8.5$ Hz, 2H, 2 × Ar-CH), 7.72 (d, $J = 8.3$ Hz, 1H, Ar-CH), 7.90 (d, $J = 8.3$ Hz, 2H, 2 × Ar-CH), 8.04 (d, $J = 8.0$ Hz, 1H, Ar-CH), 8.05 (d, $J = 8.1$ Hz, 2H, 2 × Ar-CH), 11.58 (s, 1H, NH); ^{13}C NMR (126 MHz, acetone- d_6): $\delta = 120.3, 120.5, 123.9, 124.1, 124.8, 125.9, 125.9, 126.4, 126.5, 127.6, 128.1, 128.8, 128.9$ (2 × Ar-CH), 129.0 (2 × Ar-CH), 131.1, 134.5, 134.5, 135.1, 139.2, 141.4, 145.9, 192.8; HRMS (ESI): m/z calcd for $\text{C}_{24}\text{H}_{17}\text{ClF}_3\text{NO}_3\text{S}\text{-H}^+$: 490.0540 [M-H] $^+$; found: 490.0544.

3.4.8. *N*-(3-[5-(4-chlorophenyl)penta-2,4-dienoyl]phenyl)-4-trifluoromethylbenzenesulfonamide (17)

Pale yellow solid; 16% crude; mp 178-179°C; IR (UATR) 3358 (NH, str.), 1572 (C=O, str.), 1275 (C=C, str.), 1145 (S=O, assym.), 998 (S=O, symm.) cm^{-1} ; ^1H NMR (500 MHz, acetone- d_6): $\delta = 7.18$ (d, $J = 15.6$ Hz, 1H, CH = CH-Ar), 7.23 (d, $J = 15.0$ Hz, 1H, COCH = CH), 7.24 (dd, $J = 15.6, 10.7$ Hz, 1H, CH = CH-Ar), 7.44 (d, $J = 8.5$ Hz, 2H, 2 × Ar-CH), 7.47 (d, $J = 8.5$ Hz, 1H, Ar-CH), 7.48 (dd, $J = 7.6, 4.2$ Hz, 1H, Ar-CH), 7.54 (dd, $J = 15.0, 10.7$ Hz, 1H, COCH = CH), 7.64 (d, $J = 8.5$ Hz, 2H, 2 × Ar-CH), 7.78 (d, 1H, $J = 8.5$ Hz), 7.87 (s, 1H, Ar-CH), 7.92 (d, $J = 8.4$ Hz, 2H, 2 × Ar-CH), 8.06 (d, $J = 8.4$ Hz, 2H, 2 × Ar-CH); ^{13}C NMR (126 MHz, acetone- d_6): $\delta = 120.4, 124.7, 124.9, 125.5, 126.4$ (2 × Ar-CH), 127.9, 127.9 (2 × Ar-CH), 128.8 (2 × Ar-CH), 128.9 (2 × Ar-CH), 129.7, 133.5, 134.2, 135.2, 137.9, 139.2, 140.3, 143.5, 144.4, 155.7, 188.4; HRMS (ESI): m/z calcd for $\text{C}_{24}\text{H}_{17}\text{ClF}_3\text{NO}_3\text{S}\text{-H}^+$: 490.1100 [M-H] $^+$; found: 490.1113.

3.4.9. *N*-(4-[5-(4-chlorophenyl)penta-2,4-dienoyl]phenyl)-4-trifluoromethylbenzenesulfonamide (18)

Pale yellow solid; 19% crude; mp 178-179°C; IR (UATR) 3158 (NH, str.), 1562 (C=O, str.), 1401 (C=C, str.), 1315 (S=O, assym.), 1155 (S=O, symm.) cm^{-1} ; ^1H NMR (500 MHz, acetone- d_6): $\delta = 7.16$ (d, $J = 15.6$ Hz, 1H, CH = CH-Ar), 7.21 (dd, $J = 15.6, 10.5$ Hz, 1H, CH = CH-Ar), 7.31 (d, $J = 14.8$ Hz, 1H, COCH = CH), 7.40 (d, $J = 8.7$ Hz, 1H, 2 × Ar-CH), 7.41 (d, $J = 8.7$ Hz, 1H, 2 × Ar-CH), 7.44 (d, $J = 8.5$ Hz, 1H, 2 × Ar-CH), 7.53 (dd, $J = 14.8, 10.5$ Hz, 1H, COCH = CH), 7.95 (d, $J = 8.4$ Hz, 2H, 2 × Ar-CH), 7.98 (d, $J = 8.8$ Hz, 2H, 2 × Ar-CH), 8.12 (d, $J = 8.3$ Hz, 2H, 2 × Ar-CH); ^{13}C NMR (126 MHz, acetone- d_6): $\delta = 119.8$ (2 × Ar-CH), 125.2 (2 × Ar-CH), 126.5, 127.4, 127.5 (2 × Ar-CH), 128.4, 128.5, 128.8, 128.9 (2 × Ar-CH), 129.0, 129.5 (2 × Ar-CH), 132.1, 133.7, 135.5, 138.1, 140.2, 141.4, 186.5, 192.9; HRMS (ESI): m/z calcd for $\text{C}_{24}\text{H}_{17}\text{ClF}_3\text{NO}_3\text{S}\text{-H}^+$: 490.0885 [M-H] $^+$; found: 490.0887.

3.5. *In vitro* biological evaluation

The purified diarylpentadienone analogues tested for both *in vitro* α -glucosidase and DPP-4 inhibitory evaluations were of 95–99% purity based on their respective high-performance liquid chromatography (HPLC) profiles.

3.5.1. α -Glucosidase inhibitory assay

α -Glucosidase inhibition assay was performed following a previously described method with slight modifications [51,52]. α -Glucosidase extracted from *Bacillus stearothermophilus* was used as the source of enzyme, while *p*-nitrophenyl- α -D-glucopyranoside (PNPG) and acarbose were used as a substrate and standard, respectively. A mixture of 10 μ l sample, 130 μ l phosphate buffer (pH 6.5, 30 mM), and 10 μ l enzyme in a 96 well plate was pre-incubated at room temperature for 5 min before 50 μ l of PNPG substrate solution (10 mM) was added and the reaction mixture was further incubated at room temperature for 15 min. The reaction was quenched by the addition of 50 μ l of 2 M glycine (pH 10) into the mixture. The absorbance of the liberated *p*-nitrophenol was measured at 405 nm using a spectrophotometer (Tecan Safire, Grödigg, Austria). All reactions were carried out in triplicates and the IC₅₀ measurements (> 50% inhibition) were performed in the presence of serial dilutions of tested compounds (50 to 1.53 μ M), calculated by the non-linear regression analysis using GraphPad Prism (version 8.0; GraphPad software) and expressed as mean \pm SEM. The tested samples can be in two forms of supernatants: pre- and post-centrifugation and were prepared as described by Auld et al., 2017 for the aggregation assay [45], while the pre-centrifugation supernatant of all compounds were used in *in vitro* α -glucosidase and DPP-4 inhibition assays.

3.5.2. DPP-4 enzyme assay

The DPP-4 inhibition activity was determined using a DPP-4 Inhibitor Screening Assay Kit (Cayman Chemical Inc., Michigan, USA), pre-stored at -80°C . A standard DPP-4 inhibitor, sitagliptin, was utilized as a positive control, while the Gly-Pro-Aminocoumarin (AMC) was used as a substrate. Stock solution of inhibitors were made by re-suspending each of the weighed pure solid diarylpentadienones in DMSO and diluted in an assay buffer to a final concentration of 100 μ M in each well. The final concentration of DMSO adjusted in the assay was 1%. Thirty μ l of diluted buffer (20 mM Tris-HCl, 100 mM NaCl, 1 mM EDTA, pH 8.0) and 10 μ l of compounds **1–18** (100 μ M) were mixed with 10 μ l DPP-4 (human recombinant) in a half volume 96-well white microplate. Fifty μ l of substrate was then added to the well, and the mixture was incubated for 30 min at 37°C . After incubation, the fluorescence emitted by each compound was measured at excitation wavelength of 350–360 nm and emission wavelength of 450–465 nm in a multimode microplate reader (Biotek PLUS, California, USA). All reactions were carried out in triplicates and the IC₅₀ measurements (> 70% inhibition) were performed in the presence of serial dilutions of tested compounds (100 to 6.13 μ M), calculated by the non-linear regression analysis using GraphPad Prism (version 8.0; GraphPad software) and expressed as mean \pm SEM.

3.5.3. Kinetic studies against α -glucosidase

The kinetic studies were performed on the most active **18** as previously described method [51,52] using different concentrations of substrate and compounds to determine the mode of α -glucosidase inhibition. Compound **18** with concentrations of 20.0, 15.0, 12.5, 10.0, 7.5, 5.0, 2.5 and 0 μ M was used for this kinetic analysis. Meanwhile, the concentrations of substrate were varied at 30, 20, 10, 4, 2 and 1.25 mM. A mixture of 10 μ l sample, 130 μ l phosphate buffer (pH 6.5, 30 mM), and 10 μ l enzyme in a 96 well plate was pre-incubated at room temperature for 5 min before 50 μ l of PNPG substrate solution of different concentrations was added. The absorbance was directly measured at

405 nm using a spectrophotometer (Tecan Safire, Grödigg, Austria) in interval 5 to 30 min. The type of inhibition was determined via the Lineweaver-Burk plot (the inverse of velocity (1/v) against the inverse of the substrate concentration (1/[S])) were derived from the resulting data.

3.6. *In vivo* toxicity in zebrafish embryos

3.6.1. Zebrafish husbandry and embryo collection

We obtained embryos through natural mating of either wild-type (WT) or transgenic Tg(kdrl:egfp) adult zebrafish obtained from the Laboratory of Natural Products, Universiti Putra Malaysia, and the Zebrafish Center for Disease Modeling, Korea. They were kept in a mixed male and female enclosure with a ratio of 2:3 with 14 h of light: 10 h of darkness-controlled photoperiod with ambient temperature at 28.5°C . They were fed four times a day, alternately with brine shrimp (*Artemia salina*, San Francisco Bay Brand, San Francisco, CA) and with commercial dry flake food (Sera Vipan). The embryos were collected 30 min after the onset of light, washed with distilled water, rinsed with embryo media (15 mM NaCl, 0.5 mM KCl, 1 mM MgSO₄, 0.15 mM KH₂PO₄, 0.05 mM Na₂HPO₄, 1 mM CaCl₂, 0.7 mM NaHCO₃, pH 7.0), and then incubated at 28°C . To eliminate fungal growth, the unfertilized embryos were discarded. The fertilized embryos were examined and chosen under a standard dissection microscope (SZX-12, Olympus, Tokyo, Japan). Animal experiments were conducted according to approved guidelines and regulations of the Institutional Animal Care and Use Committee (IACUC) at the Animal Ethics Committee of Universiti Putra Malaysia (IACUC/AUP-R079) and Chungnam National University.

3.6.2. Acute toxicity testing on zebrafish embryos

To test acute toxicity on early embryonic development, ten zebrafish embryos at 6 hpf were placed in each well of a 24 well plate, containing 1 ml of embryo medium. Compound **18** was dissolved in dimethyl sulfoxide (DMSO) to make a 40 mM stock solution and diluted into the embryonic water at 1, 2, 5, 10, 20, and 40 μ M concentrations. The compound solution was changed every day to maintain freshness of solutions. To acquire microscopic images, zebrafish embryos were dechorionated using forceps, anesthetized in Tricaine (Sigma-Aldrich), and mounted in 3% methylcellulose. Embryos were visualized using a Nikon AZ100 microscope (Nikon, Tokyo, Japan). Digital images were captured using a Nikon Digital Sight DS-Fil1 digital camera (Nikon) and processed with NIS-Elements F 3.0 (Nikon)

3.6.3. Evaluation of apoptosis

Evaluation of cell death in the wild-type (WT) zebrafish larvae after treatment with compound **18** was determined via a vital fluorescent dye acridine orange method that often used as a marker of apoptotic cells in zebrafish. Acridine orange staining is a rapid method and has been shown to be highly selective for apoptotic cells where determination of apoptosis was made by measuring relative acridine orange fluorescence in zebrafish embryos. Zebrafish larvae were placed in the egg water containing 4 μ g/ml of acridine orange (Sigma) for 20 min. Afterwards, the live zebrafish larvae were washed with the egg water 5 times for 5 min each, anesthetized with tricaine and mounted in 3% methylcellulose, prior examined by stereomicroscopy and fluorescent microscopy, as previously described [60,61].

3.6.4. Evaluation of adverse effect on the formation of blood vessel

Zebrafish embryos obtained from the blood vessel-specific EGFP fluorescent transgenic zebrafish line, Tg(kdrl:egfp), were treated with 0.1% dimethyl sulfoxide (DMSO) as a control or treated with various concentrations of compound **18**. Treatment with compound **18** commenced from the late gastrula stage at 10 hpf and examined at 30 hpf when normal blood vessel formation was prominent in the control

zebrafish. For bioimaging, embryos were mounted in 3% methylcellulose on a glass slide and live animal images were captured using a stereo microscope (LEICA MZ16FA) and digital camera (LEICA DFC450C).

3.6.5. Statistical analysis

Statistical analyses were performed using SPSS (SPSS v. 25.0). One-way analysis of variance (ANOVA) was used to determine the effects of each treatment groups to the control. Data were represented as mean \pm standard error mean (SEM) using GraphPad Prism (Graphpad Software, USA). The data were significantly different when $p \leq 0.05$. To assure these values were independent, the data analyzed were based on a per well basis in order to avoid any interaction biases among the embryos.

3.7. Molecular docking studies

3.7.1. Homology modelling and model verification

A three-dimensional model of *B. stearothermophilus* α -glucosidase was built by comparative modeling using the SWISS-MODEL program (automated protein structure homology-modeling server; <http://swissmodel.expasy.org>). The crystallographic structure of the related GH-13 α -glycosidase from the *Geobacillus* sp. strain HTA-462 (PDB: 2ZEO) was selected as the template due to its highest sequence identity (94%) with respect to the *B. stearothermophilus* α -glucosidase [62]. The amino acid sequence of *B. stearothermophilus* α -glycosidase (EC 3.2.1.20), which comprised of 555 amino acid residues was retrieved (GenBank accession: D84648.1; NCBI <http://www.ncbi.nlm.nih.gov>). The modeled protein was checked using the PROCHECK (stereochemical quality analysis software) program [63].

3.7.2. Ligand preparation, energy minimization and geometrical optimization

The theoretical 3D structure ligand of the most active inhibitor (compounds **15** and **18**) was firstly drawn in Chemdraw Ultra 12.0 as a 2D structure before being saved as MDL mol file. The ligand structure file was imported to Avogadro (version 1.2.0) as a 3D model and was optimized by means of energy minimization carried out with General AMBER Force Field (GAFF) force field. These ligands were prepared by assigning nonpolar hydrogens using AutoDockTools 1.5.4.

3.7.3. Docking studies and results visualization

Docking calculations were performed with the software AutodockVina. The Vina program was employed to generate the docking input files and to analyze the docking results. The proteins were considered rigid. The final output of the docking procedure was a set of solutions ranked according to their corresponding scoring function values, each defined by the 3D coordinates of its atoms. The Discovery studio visualizer 4.0 (Accelrys, San Diego, USA) was used to visualize and analyze the results. For *Homo sapiens*-sourced of α -glucosidase, the X-ray coordinates of human lysosomal acid- α -glucosidase, GAA, in complex with acarbose (PDB code: 5NN8, resolution = 2.45 Å) was retrieved and treated as discussed above for file preparation.

Declaration of Competing Interest

The authors declare that they have no known competing financial interests or personal relationships that could have appeared to influence the work reported in this paper.

Acknowledgement

The authors would like to acknowledge Universiti Putra Malaysia for their financial support under the Putra grant – Putra Young Initiative (IPM) with sponsorship reference number GP-IPM/2016/

9480700 and grant from the Korean Ministry of Trade, Industry and Energy (10063396 to C.H.K.)

Appendix A. Supplementary data

Supplementary data to this article can be found online at <https://doi.org/10.1016/j.bioorg.2020.104277>.

References

- [1] G. Roglic, *Int. J. Noncomm. Diseases*. 1 (2016) 3–8.
- [2] K.G.M.M. Alberti, P.F. Zimmet, *Diabetic Med.* 15 (1998) 539–553.
- [3] D. Atlas, International diabetes federation. IDF Diabetes Atlas, 7th edition., International Diabetes Federation, Brussels, Belgium, 2015.
- [4] S.H. Havale, M. Pal, *Bioorg. Med. Chem.* 17 (2009) 1783–1802.
- [5] S. Matthaehi, R. Bierwirth, A. Fritsche, B. Gallwitz, H.U. Häring, H.G. Joost, M. Kellner, C. Kloos, T. Kunt, M. Nauck, G. Scherthaner, *Exp. Clin. Endocrinol. Diabetes*. 117 (2009) 522–557.
- [6] E.Y. Lee, S. Kaneko, P. Jutabha, X. Zhang, S. Seino, T. Jomori, N. Anzai, T. Miki, *J. Endocrinol.* 224 (2015) 205–214.
- [7] Alpha Glucosidase Inhibitors (2020, June 2). Retrieve from <https://www.diabetes.co.uk/diabetes-medication/alpha-glucosidase-inhibitors.html>.
- [8] C.H. McIntosh, *Can. J. Diabetes*. 32 (2008) 131–139.
- [9] K. Makrilakis, *Int. J. Environ. Res. Public Health*. 16 (2019) 2720–2739.
- [10] A.K. Singh, *Indian J. Endocrinology Metab.* 18 (2014) 753–760.
- [11] S.L. Gaonkar, U.N. Vignesh, *Res. Chem. Intermed.* 43 (2017) 6043–6077.
- [12] C. Zhuang, W. Zhang, C. Sheng, W. Zhang, C. Xing, Z. Miao, *Chem. Rev.* 117 (2017) 7762–7810.
- [13] Z. Rozmer, P. Perjési, *Phytochem. Rev.* 15 (2016) 87–120.
- [14] D.I. Batovska, I.T. Todorova, *Curr. Clin. Pharmacol.* 5 (2010) 1–29.
- [15] B. Orlikova, D. Tasdemir, F. Golais, M. Dicato, M. Diederich, *Genes Nutr.* 6 (2011) 125–147.
- [16] H. Sun, D. Wang, X. Song, Y. Zhang, W. Ding, X. Peng, X. Zhang, Y. Li, Y. Ma, R. Wang, P. Yu, *J. Agric. Food Chem.* 65 (2017) 1574–1581.
- [17] Y.C. Hu, Y.D. Luo, L. Li, M.K. Joshi, Y.H. Lu, *J. Agric. Food Chem.* 60 (2012) 10683–10688.
- [18] X.W. Yang, M.Z. Huang, Y.S. Jin, L.N. Sun, Y. Song, H.S. Chen, *Fitoterapia*. 83 (2012) 1169–1175.
- [19] A.T. Bale, K.M. Khan, U. Salar, S. Chigurupati, T. Fasina, F. Ali, A. Kanwal, M. Wadood, S.S. Taha, M. Nanda, S.P. Ghufuran, *Bioorg. Chem.* 79 (2018) 179–189.
- [20] F. Jabeen, P.V. Oliferenko, A.A. Oliferenko, G.G. Pillai, F.L. Ansari, C.D. Hall, A.R. Katritzky, *Eur. J. Med. Chem.* 80 (2014) 228–242.
- [21] C.Y. Cai, L. Rao, Y. Rao, J.X. Guo, Z.Z. Xiao, J.Y. Cao, Z.S. Huang, B. Wang, *Eur. J. Med. Chem.* 130 (2017) 51–59.
- [22] F.L. Ansari, S. Umbreen, L. Hussain, T. Makhmoor, S.A. Nawaz, M.A. Lodhi, S.N. Khan, F. Shaheen, M.I. Choudhary, *Chem. Biodivers.* 2 (2005) 487–496.
- [23] H. Sun, Y. Li, X. Zhang, Y. Lei, W. Ding, X. Zhao, H. Wang, X. Song, Q. Yao, Y. Zhang, Y. Ma, R. Wang, T. Zhu, P.Y. Bioorg. Med. Chem. Lett. 25 (2015) 4567–4571.
- [24] H.W. Ryu, B.W. Lee, M.J. Curtis-Long, S. Jung, Y.B. Ryu, W.S. Lee, K.H. Park, *J. Agric. Food Chem.* 58 (2010) 202–208.
- [25] W.D. Seo, J.H. Kim, J.E. Kang, H.W. Ryu, M.J. Curtis-Long, H.S. Lee, M.S. Yang, K.H. Park, *Bioorg. Med. Chem. Lett.* 15 (2005) 5514–5516.
- [26] A.S. Kalgutkar, R. Jones, A. Sawant, Chapter 5: Sulfonamide as an essential functional group in drug design, in: D.A. Smith (Ed.), *Metabolism, Pharmacokinetics and toxicity of Functional Groups: Impact of Chemical Building Blocks on ADMET*, Cambridge, RSC Publishing, 2010, pp. 210–273.
- [27] I.M. Prlina, C.P. Dahlen, A.J. Bischoff, *Antibiot. Med. Clin. Ther. (New York, NY)*. 5 (1958) 242–250.
- [28] B.P. Ryan, *M. J. Australia*. 1 (1975) 101–103.
- [29] W.W. Douglas, R.P. Rubin, *J. Physiol.* 159 (1961) 40–57.
- [30] A. Markham, *Drugs*. 77 (2017) 697–704.
- [31] J.C. Adkins, D. Faulds, *Drugs*. 55 (1998) 837–842.
- [32] P. Chen, D. Feng, X. Qian, J. Apgar, R. Wilkening, J.T. Kuethe, Y.D. Gao, G. Scapin, J. Cox, G. Doss, G. Eiermann, *Bioorg. Med. Chem. Lett.* 25 (2015) 5767–5771.
- [33] S. Rocha, A. Sousa, D. Ribeiro, C.M. Correia, V.L.M. Silva, C.M.M. Santos, A.M.S. Silva, A.N. Araujo, E. Fernandes, M. Freitas, *Food Funct.* 10 (2019) 5510–5520.
- [34] Z. Wang, Sen, L.Z. Cheng, H.P. Zhou, X.H. Liu, F.H. Chen, *Bioorg. Med. Chem. Lett.* 27 (2017) 1803–1807.
- [35] J.A.Q. Suarez, D.G. Rando, R.P. Santos, C.P. Gonçalves, E. Ferreira, J.E. de Carvalho, L. Kohn, D.A. Maria, F. Faião-Flores, D. Michalik, M.C. Marcucci, *Bioorg. Med. Chem.* 18 (2010) 6275–6281.
- [36] D.J. Weldon, M.D. Saulsbury, J. Goh, L. Rowland, L. Robinson, C. Miller, J. Christian, L. Amis, N. Taylor, C. Dill, *Bioorg. Med. Chem. Lett.* 24 (2014) 3381–3384.
- [37] D. Batovska, S. Parushev, B. Stamboliyska, I. Tsvetkova, *Eur. J. Med. Chem.* 44 (2009) 2211–2218.
- [38] C. Conti, P. Mastromarino, P. Goldoni, G. Portalone, N. Desideri, *Antiviral Chem. Chemother.* 16 (2005) 267–276.
- [39] S. Das, I. Mitra, S. Batuta, M.N. Alam, K. Roy, N.A. Begum, *Bioorg. Med. Chem. Lett.* 24 (2014) 5050–5054.
- [40] G.M. Rishon, *Drug Disc. Today*. 8 (2003) 86–96.

- [41] K.E. Coan, B.K. Shoichet, *J. Am. Chem. Soc.* 130 (2008) 9606–9612.
- [42] D. Lagorce, L. Bouslama, J. Becot, M.A. Miteva, B.O. Villoutreix, *Bioinform.* 33 (2017) 3658–3660.
- [43] J.J. Irwin, D. Duan, H. Torosyan, A.K. Doak, K.T. Ziebart, T. Sterling, G. Tumanian, B.K. Shoichet, *J. Med. Chem.* 58 (2015) 7076–7087.
- [44] L.G. Viviani, E. Piccirillo, A. Cheffer, L. de Rezende, H. Ulrich, A.M. Carmona-Ribeiro, A.T. Amaral, *Molecules.* 23 (2018) 876–1890.
- [45] D. S. Auld, J. Inglese, J. L. Dahlin, Assay Interference by Aggregation. 2017 Jul 26. In: G. S. Sittampalam, A. Grossman, K. Brimacombe, Assay Guidance Manual [Internet]. Bethesda (MD): Eli Lilly & Company and the National Center for Advancing Translational Sciences; 2004. Available from: <https://www.ncbi.nlm.nih.gov/books/NBK442297/>.
- [46] S.L. McGovern, B.T. Helfand, B. Feng, B.K. Shoichet, *J. Med. Chem.* 46 (2003) 4265–4272.
- [47] J.B. Baell, J.W.M. Nissink, *ACS Chem. Biol.* 13 (2018) 36–44.
- [48] C. Aldrich, C. Bertozi, G.I. Georg, L. Kiessling, C. Lindsley, D. Liotta, K.M. Merz Jr, A. Schepartz, S. Wang, *ACS Chem. Neurosci.* 8 (2017) 420–423.
- [49] J.B. Baell, G.A. Holloway, *J. Med. Chem.* 53 (2010) 2719–2740.
- [50] D.N. Dhar, J.B. Lal, *J. Org. Chem.* 23 (1958) 1159–1161.
- [51] J.S. Kim, C.S. Kwon, K.H. Son, *Biosci. Biotechnol. Biochem.* 64 (2000) 2458–2461.
- [52] B. Sarmadi, F. Aminuddin, M. Hamid, N. Saari, A. Abdul-Hamid, A. Ismail, *Food Chem.* 134 (2012) 905–911.
- [53] C.R. Garcia, P.D. Noyes, R.L. Tanguay, *Pharmacol. Ther.* 16 (2016) 11–21.
- [54] C.A. MacRae, R.T. Peterson, *Nat. Rev. Drug Discov.* 14 (2015) 721–731.
- [55] R.L. Tanguay, *Toxicol. Sci.* 163 (2018) 3–4.
- [56] L.K. Cole, L.S. Ross, *Dev. Biol.* 240 (2001) 123–142.
- [57] B.M. Weinstein, N.D. Lawson, *Cold Spring Harb Symp Quant Biol.* 67 (2002) 155–162.
- [58] O. Cleaver, P.A. Krieg, Molecular mechanisms of vascular development, in: R.P. Harvey, N. Rosenthal (Eds.), *Heart Development*, San Diego, Academic Press, 1999, pp. 221–252.
- [59] N.U. Rehman, K. Rafiq, A. Khan, S.A. Halim, L. Ali, N. Al-Saady, A.H. Al-Balushi, H.K. Al-Busaidi, A. Al-Harrasi, *Mar. Drugs.* 17 (2019) 666–680.
- [60] Y.M. Jeong, T.E. Jin, J.H. Choi, M.S. Lee, H.T. Kim, K.S. Hwang, D.S. Park, H.W. Oh, J.K. Choi, V. Korzh, M. Schachner, K.H. You, C.H. Kim, *J. Genet. Genomics.* 41 (2014) 583–589.
- [61] H.T. Kim, J.H. So, S.H. Jung, D.G. Ahn, W. Koh, N.S. Kim, S.H. Kim, S. Lee, C.H. Kim, *BMC Dev. Biol.* 11 (2011) 49–56.
- [62] T. Shirai, V.S. Hung, K. Morinaka, T. Kobayashi, S. Ito. *Proteins: Struct. Funct. Bioinf.* 73 (2008) 126–133.
- [63] R.A. Laskowski, J.A.C. Rullmann, M.W. MacArthur, R. Kaptein, J.M. Thornton, *J. Biomol. NMR.* 8 (1996) 477–486.